# II Mechanical and Optical Design of the EMC

## II.1 Overview of the Mechanical and Optical Systems

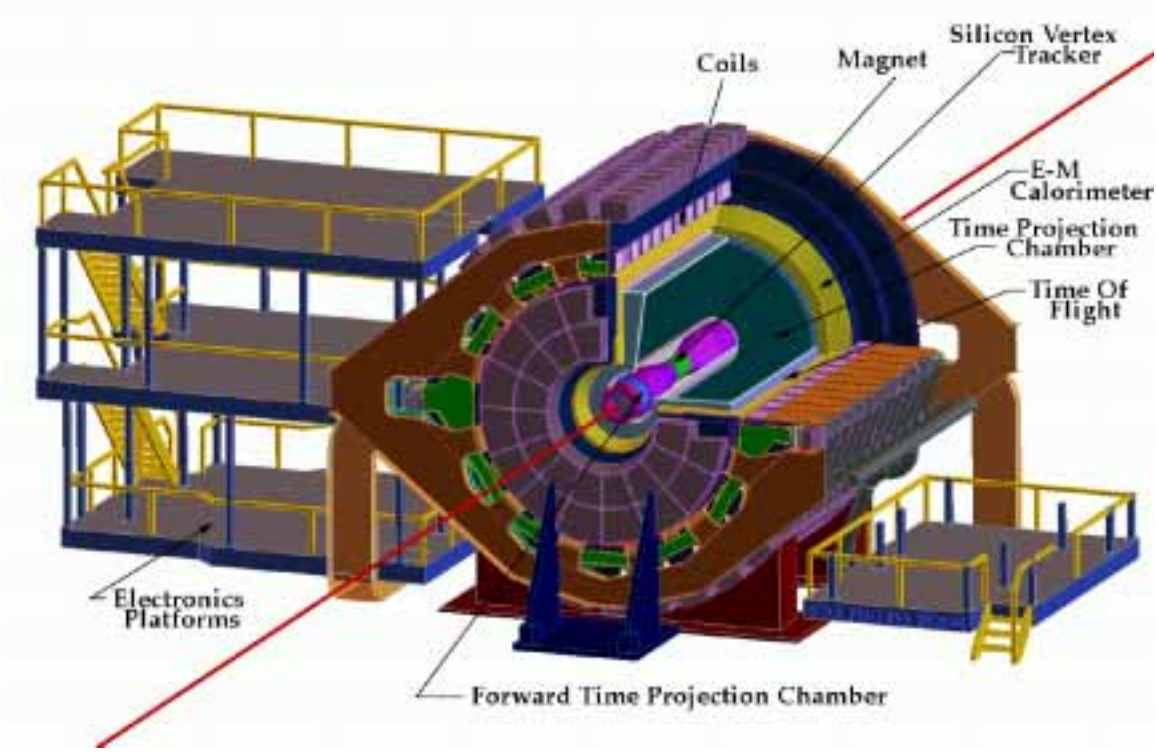


Figure II.1-1. Schematic illustration of the STAR detector showing the location of the EMC within the coils of the room temperature magnet, and the electronics boxes located on the outside of the magnet.

The overall design of the EMC has been heavily influenced by its location within the STAR detector, and hence it is helpful to review this location before explaining in detail the EMC's design. Figure II.1-1 shows a schematic illustration of the STAR detector at RHIC showing the principle sub-systems and the calorimeter. The EMC is located inside the large room temperature magnet within a cylindrical space approximately 41cm deep, by 6.2m in length, sandwiched between the Time of Flight system and the magnet coils. Due to the adverse affects of the magnetic field on the PMTs, they must be situated outside the magnet in the electronics boxes which are mounted on the flux return bars, or magnet backlegs, along with the rest of the associated readout electronics. Optical fibers run through the magnet coils to connect the EMC to its readout electronics.

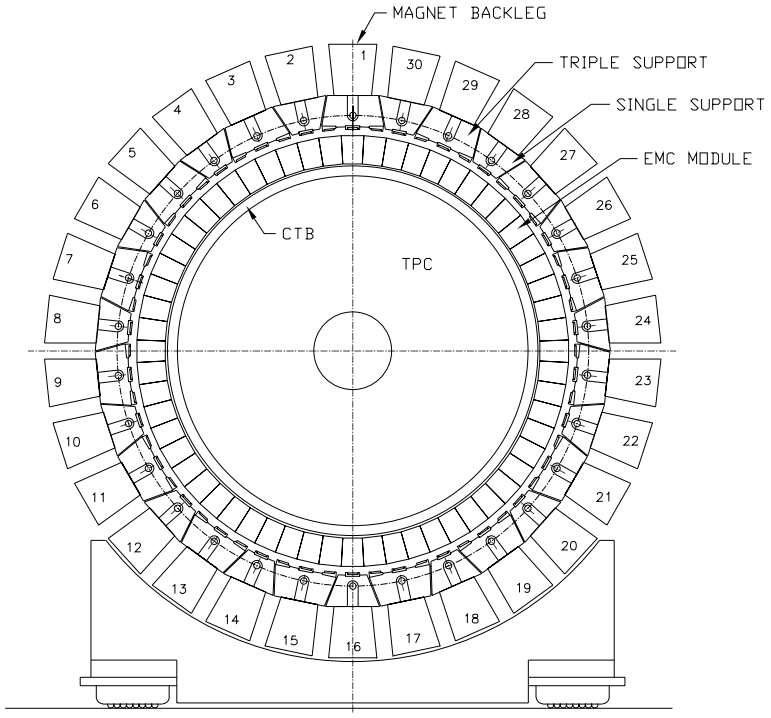


Figure II.1-2. End view of the EMC showing 60 modules, 30 flux return bars, and the alternating pattern of EMC support segments (single and triple).

The design for the barrel electromagnetic calorimeter includes a total of 120 calorimeter modules, each subtending 6° in $\Delta\phi$ (0.1 radian) and 1.0 unit in $\Delta\eta$. These modules are mounted 60 in $\phi$ by 2 in $\eta$ as shown in Fig II.1-2.

Each module is roughly 26cm wide by 293cm long with an active depth of 23.5cm plus about 6.6 cm in structural plates. A module is further segmented into 40 towers, 2 in $\phi$ and 20 in $\eta$, with each tower being 0.05 in $\Delta\phi$ by 0.05 in $\Delta\eta$. The calorimeter is thus physically segmented into a total of 4800 towers. Figure II.1-3 shows a side view of a module illustrating the projective nature of the towers in the $\eta$-direction, pointing back to the interaction region in the center of the barrel.

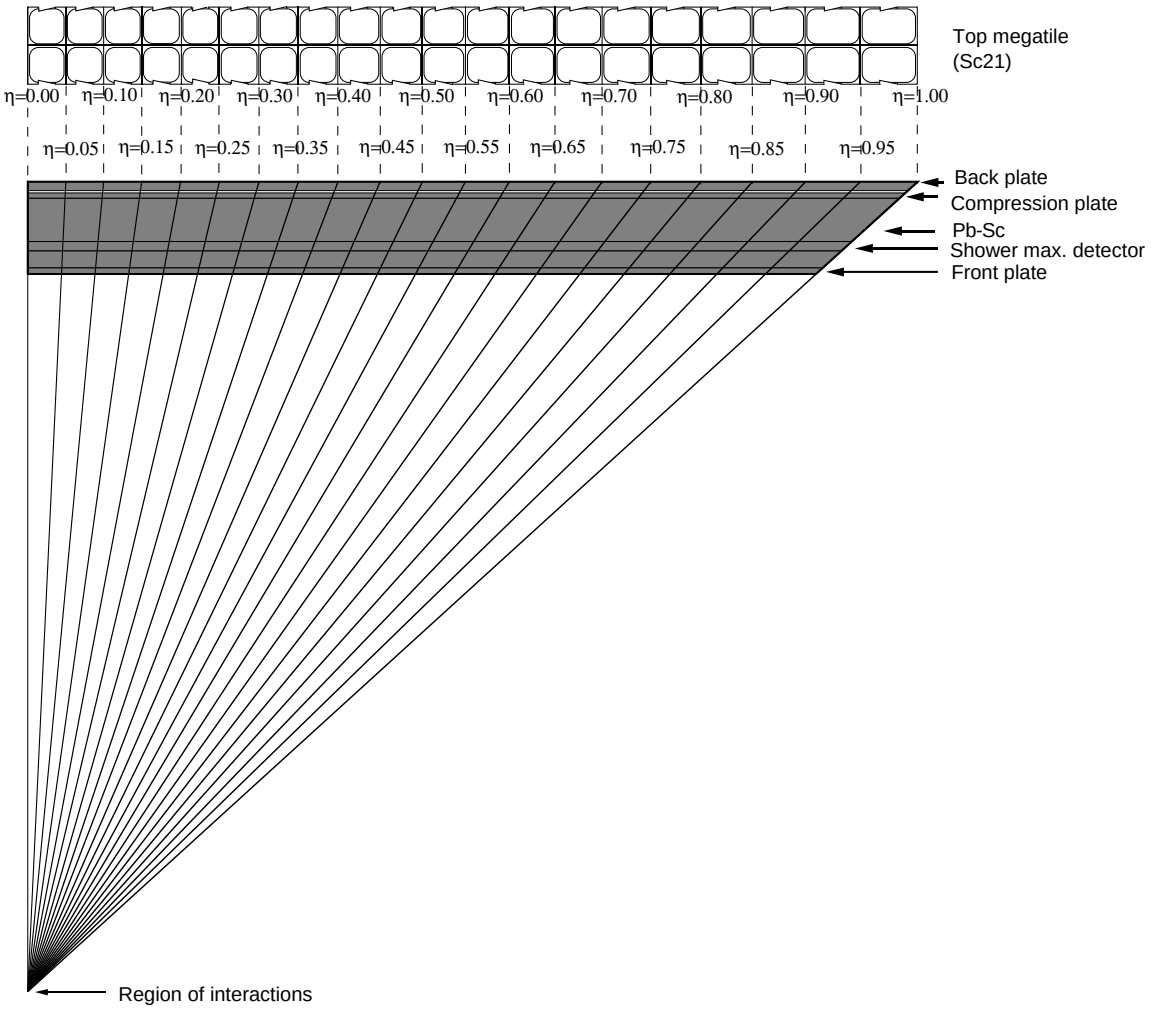


Figure II.1-3. Side view of a calorimeter module showing the projective nature of the towers. The 21st megatile layer is also shown.

The calorimeter is a sampling calorimeter, and the core of each structure consists of a lead-scintillator stack and a shower maximum detector situated approximately 5 radiation lengths from the front of the stack. There are 20 layers of 5mm thick lead and 21 layers of 5mm thick scintillator. This core structure, the stack, is held together by friction in the presence of compressional forces applied to the module stack. The compression is applied by a combination of 30 straps connecting the front and back plates of the structure, and a system of bolts and spring loaded washers between the back plate and a compression plate, as discussed in detail in section II.2.

The plastic scintillator is in the form of “megatiles”, with 40 optically isolated “tiles” in each layer as shown in figure II.1-3. The true projective nature of the towers (constant size in $\Delta\phi$ and $\Delta\eta$) means that there are 420 different tile sizes in the calorimeter. This makes alternative scintillator production techniques such as injection molding impractical. In order to simplify handling, the megatiles are produced from two pieces of approximately 1.6 m long scintillating plates for each layer in the calorimeter. The signal from each scintillating tile is read-out with a wavelength shifting (WLS) fiber embedded

in a σ-groove that is machined in the tile as shown in figure II.1-4. After exiting the scintillator, the WLS fiber is routed along the side of the stack and terminated at a multi-fiber optical connector at the back-plate of module. 3.5 m long multi-fiber optical cables of clear fibers carry the light from the optical connector through the magnet structure to the electronics boxes mounted on the magnet backlegs where the PMT′s are located. Here the light from each of the tiles composing a tower is merged via a light mixer, which is placed between the fibers and the photocathode of the PMT to optimize detection uniformity.

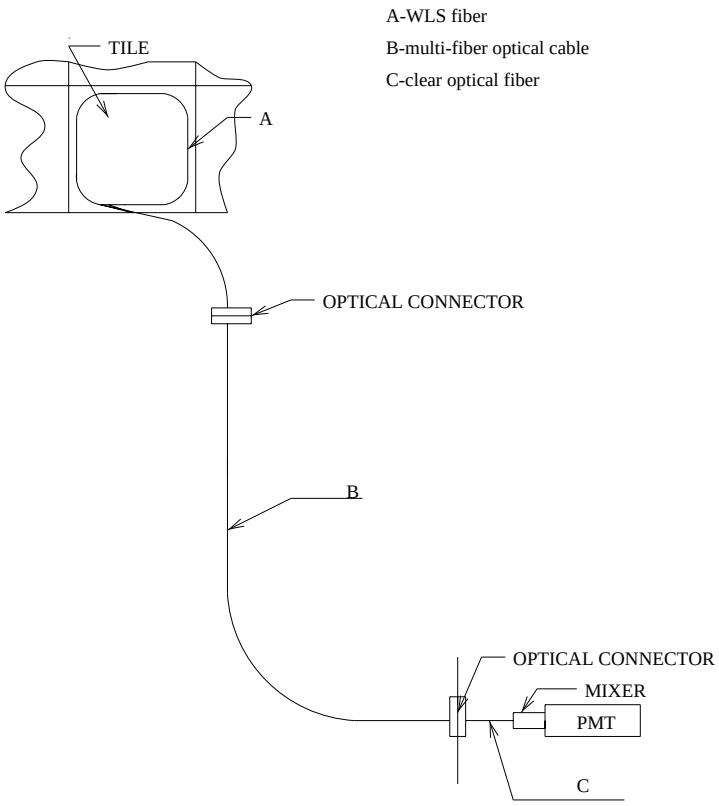


Figure II.1-4. A schematic illustration of the optical readout system for the EMC. The scintillator tile is readout by a short WLS fiber (A), which is coupled via a fiber ribbon cable (B), to the electronics boxes. Inside the electronics boxes the fibers are arranged into bundles corresponding to towers, by the clear fiber pigtails (C). The bundles then couple to the PMTs by light mixers.

The funding profile of the EMC is significantly delayed relative to the rest of STAR. This means that the calorimeter modules will be fabricated and installed into the magnet after the TPC and Central Trigger Barrel (and the initial implementation of the Time of Flight system) have been installed. In order to avoid removing the TPC during the EMC installation process, each EMC module is mounted on five sets of linear bearings which allow it to slide parallel to the axis of the magnet on linear rail systems which are anchored to the flux return bars. Part of the magnet, the linear rails systems, and the module, are shown in figure II.1-5. The linear rail systems themselves are each mounted to the magnet via five support segments, located between the magnet coils, which allow

the load of the calorimeter to be cantilevered back to the flux return bars of the magnet. The support segments have to be large enough to span the radial distance of the coils. Figure II.1-2 shows an end view of the magnet, illustrating the support segments and rail systems.

The readout fibers of the calorimeter have to be routed through the gaps between the coils. To facilitate this, vacuum-formed plastic fiber guides are inserted into the support segments. These allow the fiber cables to be pulled through the five gaps between the magnet coils at the same time as the module is slid into the magnet on its linear bearings. Cables from the wire-strip gas shower max detector situated in the stack at approximately 5 $X_o$ are routed out of the module at the $\eta$=1 end of the detector.

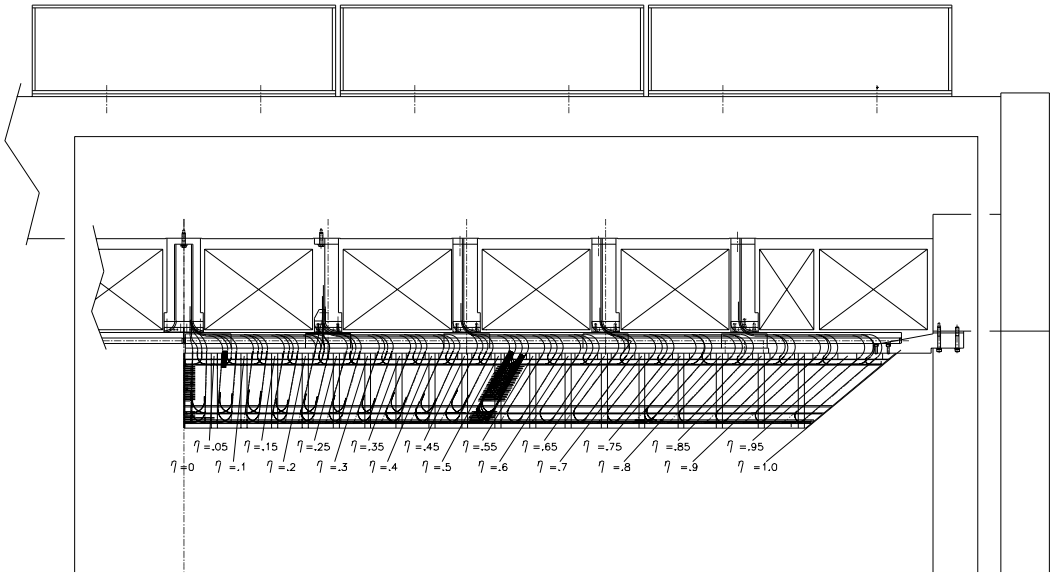


Figure II.1-5. Side view of an EMC module showing the scheme of routing the optical fibers between the coils of the magnet and the scheme of fiber routing on the sides of the module.

The mechanical and optical structure of the detector will be described in detail in the following sections, along with the research and development leading to verification of its design.

## II.2 The Mechanical Design of the EMC Module

### II.2.1 Compressed Module Design

The barrel electromagnetic calorimeter is composed of 120 calorimeter modules, each spans 6 degrees in azimuth and 1.0 in $\Delta\eta$. The 120 modules are located inside the aluminum coil of the STAR solenoid and are physically attached to the magnet flux return bars through sets of supports segments. These segments are alternately distributed in azimuth as “singles” (holds one module), and “triples” (holds three modules), as shown in Fig II.2.1.1. There are 30 flux return bars in the magnet, consequently there are 15 single and 15 triple supports on the same radius-phi plane. In the direction of the solenoid axis, the segments are distributed along the flux return bars in the spaces between coils. There are 9 segments total per flux return bar, one at the center that holds the eta=0 end

of two adjacent modules and 4 following in each opposite direction (Fig. II.2.1-2.) The center segments are distributed in azimuth in the radius-phi plane that intersects eta=0, dividing the barrel in two equal halves. On each half, linking the segments that runs along each flux return bar there is a double track for precision linear bearings that allows the modules to be slid into their final positions in the detector (Fig. II.2.1-2).

A compressed design has been adopted for the modules. The structural members of each module are: an aluminum back plate 31.7 mm thick, an aluminum front plate 19 mm thick, 30 stainless steel type 316 straps 2 mm thick and two stainless steel type 316 bulkheads 4.75 mm thick each. The back and front plates are held together at the proper boundary dimensions by the uniform distribution of the 30 straps and two bulkheads plates. The straps are mounted, 15 on each side of the module, and the bulkheads, one at eta = 0 and one at eta = 1 (Fig II.2.1.3). These straps, and bulkheads in particular, align the back and front plates and serve to resist the compressive force applied to the stack. On the outside face of the back plate is attached an aluminum interface plate 25 mm thick, 193 mm wide and just under the length of the module. This plate interfaces the back plate with a set of five linear bearing carriages. These carriages mate with the tracks mounted on the support segments, and are distributed along the back plate such that they align with the support segments when the module is fully inserted (Fig. II.2.1.2).

The dimensions of the module in the eta direction are 2930.4 mm (maximum length of the back plate) and 2574.3 mm (minimum length of the front plate). In the phi direction, the dimensions are 259.9 mm (maximum width of the back plate) and 228.1mm (minimum width of the front plate). In the radial direction the depth is 302.9 mm. The radius from the front plate to the central axis of the magnet is 2235 mm. The gap between two modules in phi is 5.6 mm cover to cover as shown in fig. II.2.1.4. The analysis of this gap and its relation to the module and rail system tolerances is discussed in chapter VIII.

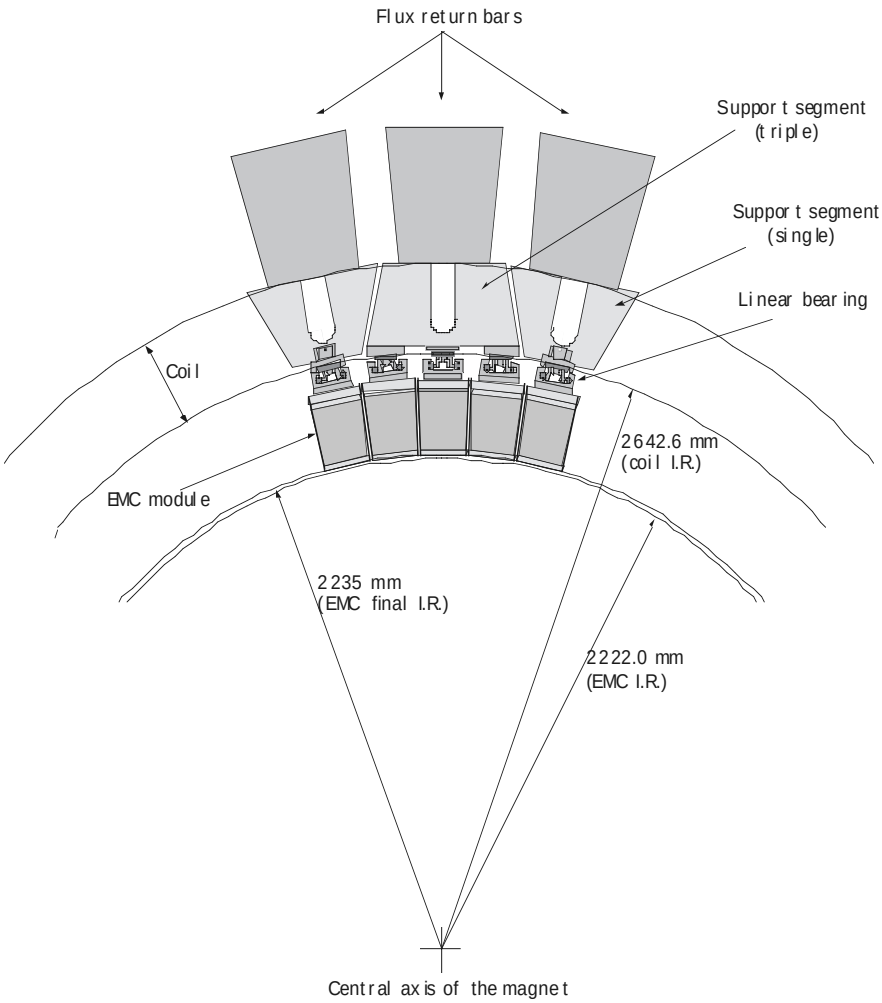


Figure II.2.1-1 Schematic illustration of the distribution of components and some radial boundaries in the barrel.

This is a lead-scintillatorsampling calorimeter. The mechanical construction of each module consists of 20 layers of 5 mm thick antimonial lead (1% Sb), 21 layers of 5 mm thick scintillator tiles, a ~ 20 mm thick SMD. Also a ~31 mm thick aluminum back plate, a ~19 mm thick aluminum compression plate and a~19 mm thick aluminum front plate. The order of components on the assembled stack is shown in Fig II.2.1-5. The scintillator layers consists of sheets called megatiles with two half megatiles making the length of a layer in the module. Individual optically isolated tiles are machined in the megatiles to obtain the 40 tiles required per layer. The tiles are sized to make the 40 projective towers in a module. The 40 towers in a module are arranged in two rows of 20 tiles of 0.05 by .05 in $\phi$ and $\eta$ running along the eta axis.

Destructive tests have been performed to determine the bending strength of the scintillator tiles with the separation grooves in place filled with epoxy, the conclusion is that failure happens in the scintillator-epoxy interface at a bending radius of 11 m implying that the tiles will be quite robust in relation to the handling they receive during module assembly.

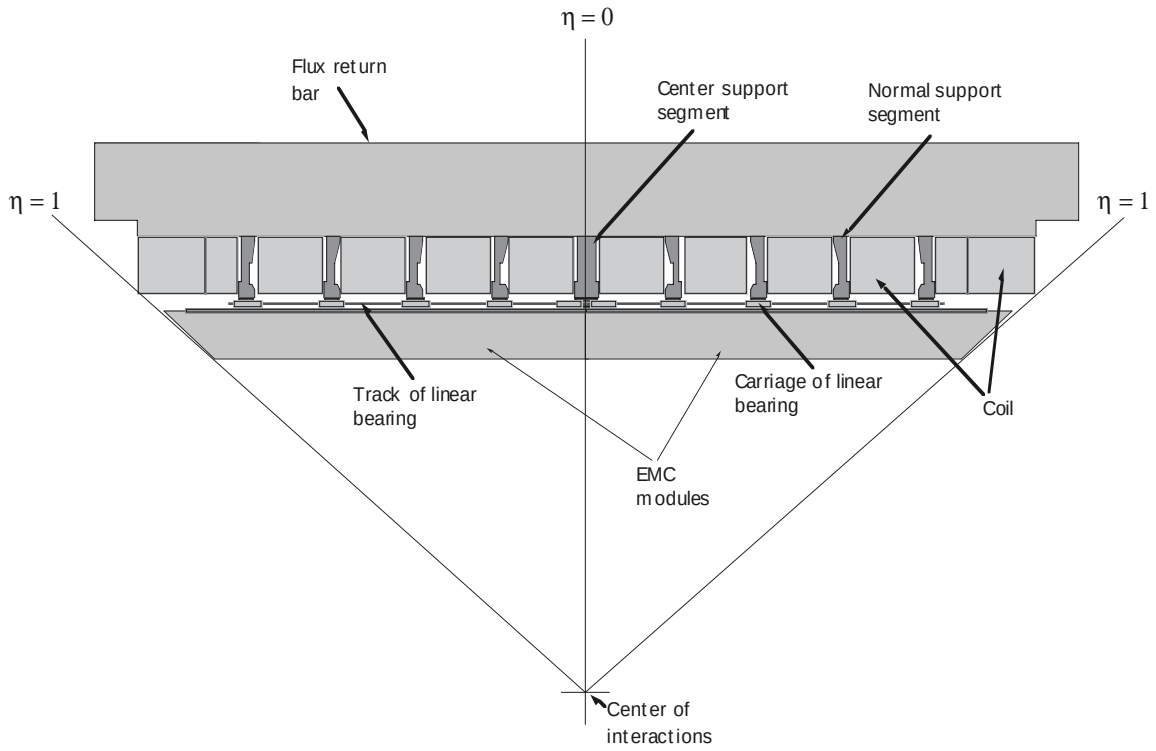


Figure II.2.1-2 Schematic illustration of one flux return bar and components linking the modules.

The wavelength shifting fibers come out at the border of each tile at a position correspondent to the eta center of the loop. This fibers are routed in the direction of the back plate where, through connectors mounted in this plate, they are connected to clear fibers. The pattern of fiber routing and connectors is shown in fig II.2.1-6.

Special care has been taken with the selection of materials used for the constru c-tion of the modules. Magnetic materials, in particular, which could distort the magnetic field of the STAR solenoid have been studied in detail. Some cases materials are used in the design. For example, the linear bearings system rods require the high strength and surface hardness of steel. Before any magnetic materials were used, however, the STAR magnet group was consulted for its approval. Where possible, of course, aluminum and stainless steel type 316 has been selected.

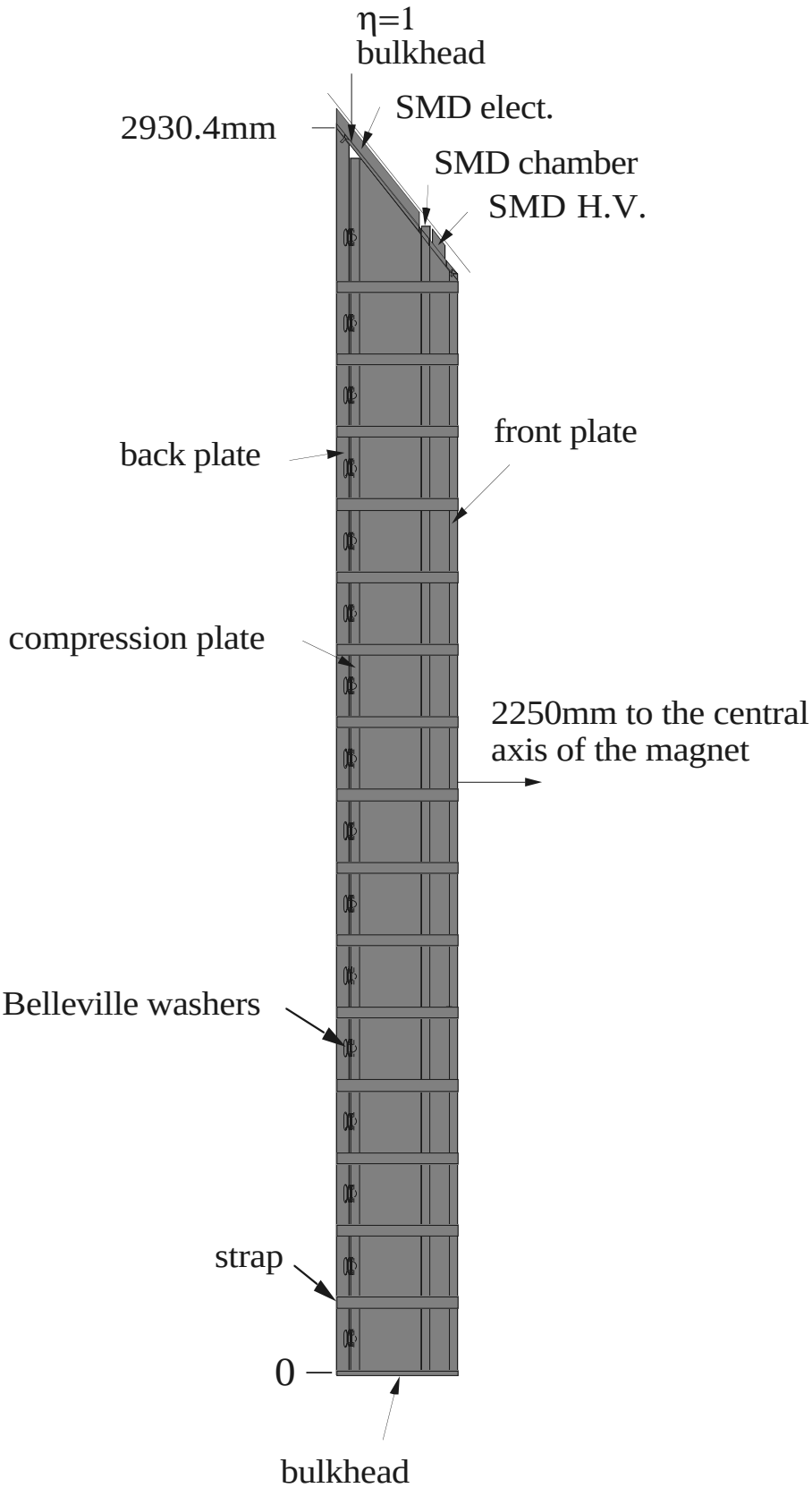


Figure II.2.1-3 Schematic illustration of the side view of the module showing components distribution.

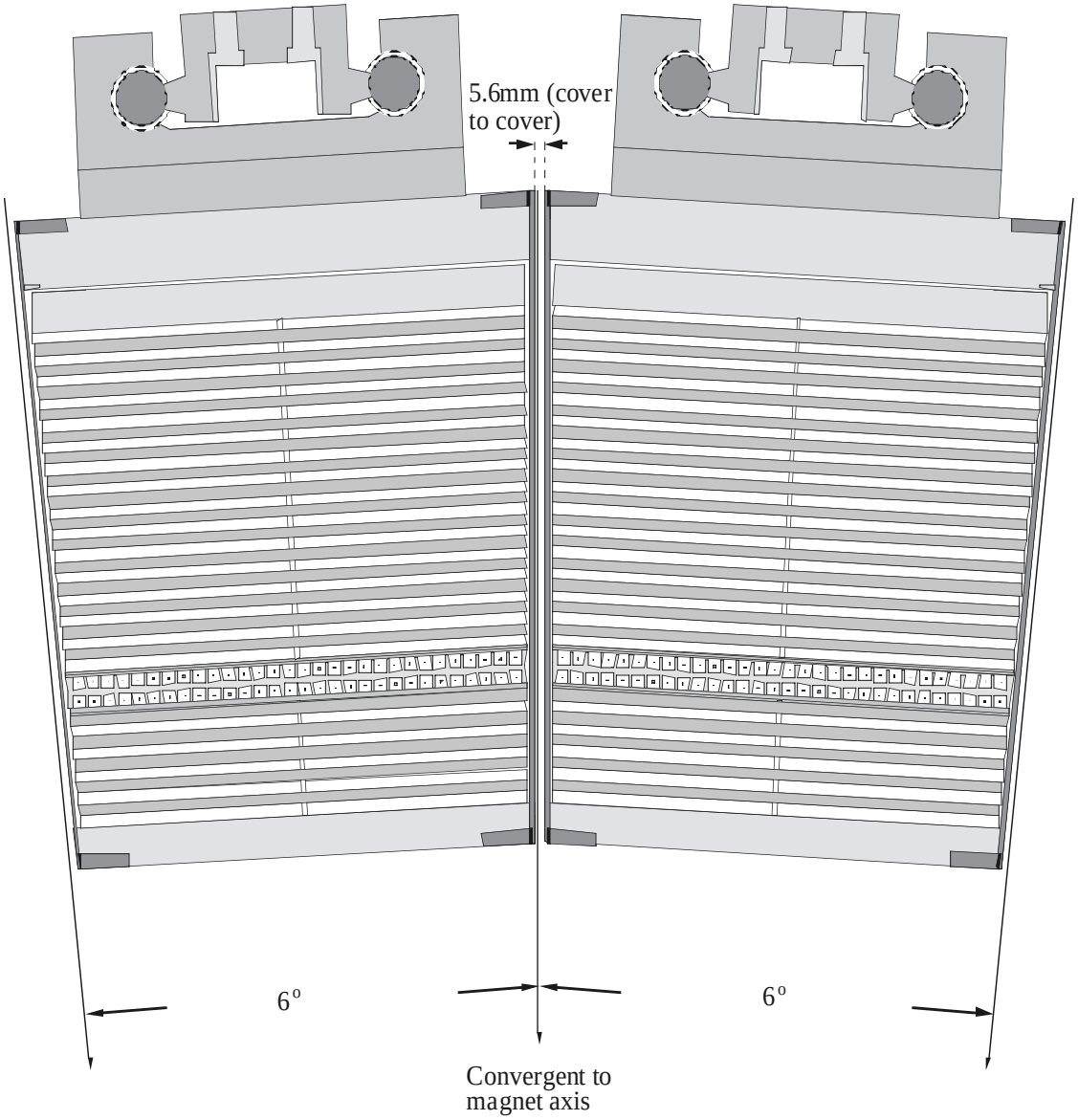


Figure II.2.1-4 View of two EMC modules showing the phi gap.

The weight of each module is ~2116 lb. and the different components of the stack are held in place by the friction that appears when a compressive force is applied between the front and compression plates. Extensive tests have been performed at WSU to determine the coefficient of static friction for every pair of materials in the stack. The minimum coefficient found was $\mu = 0.25$ corresponding to the bond paper-scintillator interface using Bicron scintillator material. Using the Russian scintillator material with its rougher surface chosen for the EMC, we find $\mu = 0.360$. Allowing a safety factor of

two and using the smaller coefficient, the compressive force needed for the stability of the stack is 2116 lb / 0.125 = 16,928 lb.

The pressure in the stack has significant variations, being ~18.7 psi on the scintillator closest to the front plate (Sc1) and~15.5 psi on the closest to the back plate (Sc21). The average pressure in the stack is ~17.1 psi.

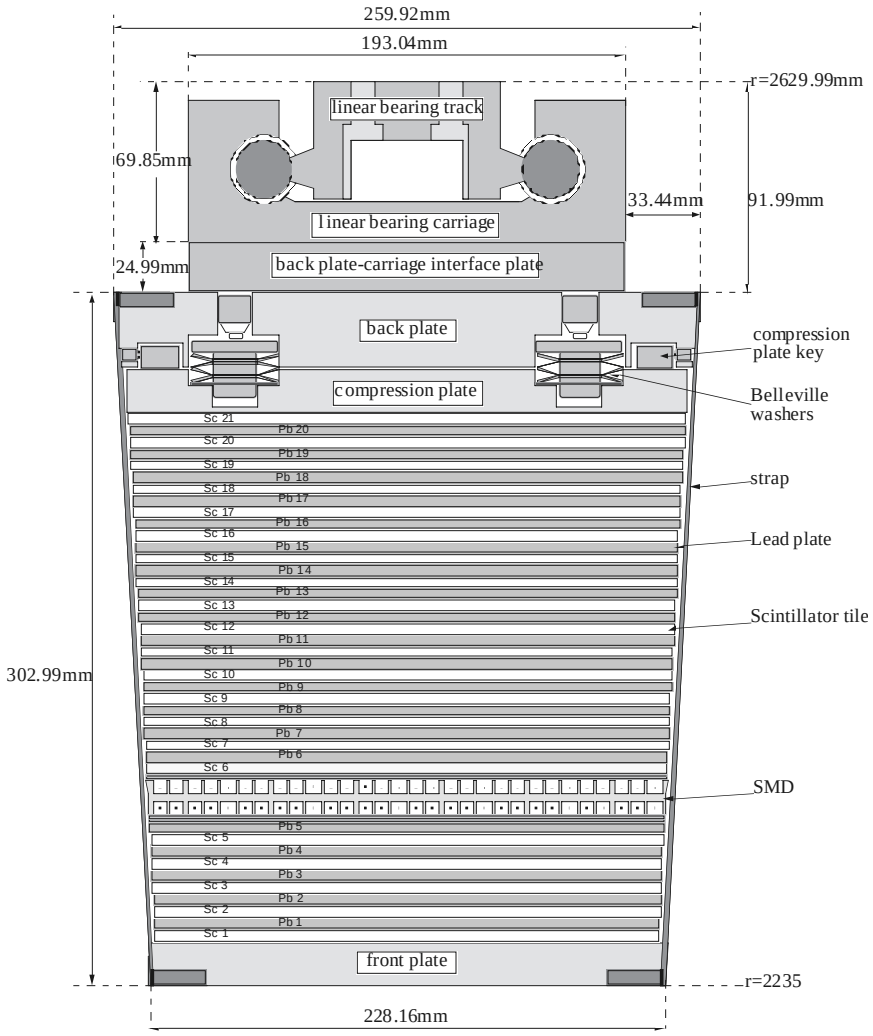


Figure II.2.1-5 Schematic illustration of a cross-section through a STAR EMC module.

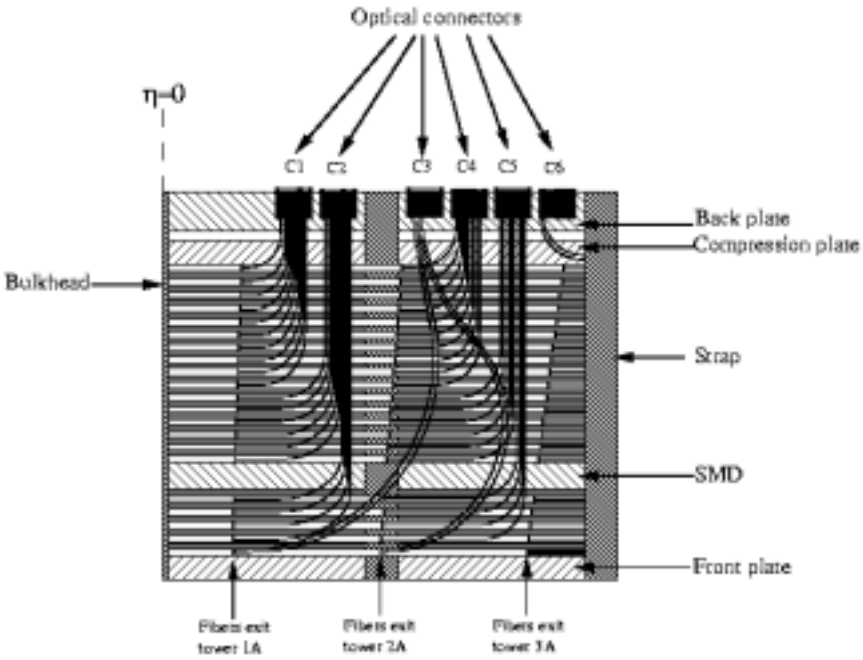


Figure II.2.1-6 Schematic view of the fiber routing at the low eta end of the module.

The required compressive force is transferred to the stack through the compression plate. This is a 19 mm thick aluminum tooling plate that is situated between the back plate and the stack. This plate receives the load from 32 sets of Belleville washers compressed by setscrews from the back plate or alternatively through 32 load cells immediately adjacent to the Belleville washers and pressed by setscrews from the back plate. The detail is shown in fig. II.2.1-7. Sensotec miniature load cell-amplifier matching sets are used for the pressure test of the prototypes and assembly of the production modules.

After stacking, the module is gradually compressed through the 32 load cells allowing the pressure to be gradually raised in a uniform fashion. After the module is stable under pressure, as indicated by readings of the load cells, the compressive force is transferred to the adjacent set of set screws which apply their force to the compression plate through Belleville washers. In this last step, the load cells are "zeroed" out in a uniform fashion preserving the uniform compression of the stack. Once the force has been transferred off of the load cells, the are removed from the stack.

Finite element analysis has been performed to study the distribution of stresses and deflections sustained by the different components of the module. Models were prepared for the $\phi$-r and $\eta$-r planes. The results of the analysis (Fig. II.2.1-8/9) show the extent of the non uniform distribution of stress in the stack that follows from the periodic placement of the straps and Belleville washer compression points. This flow generates a higher stress (~40 psi) along the stack concentrated in an area adjacent to the $\phi$ boundary and decreasing towards the center of the module to a pressure < 10 psi. To verify the results of the analysis, the stack was assembled with Prescale (pressure sensitive film) installed. The film was placed close to the front plate, at the center and close to the com-

pression plate. A combination of films and special pads was used to cover the range from 0 to 75 psi. The results of the Prescale film test validated qualitatively the FEA calculations. The FEA calculations which were performed primarily to examine the stress distribution in the scintillator (see below) have also shown that the stress and deflections on all the mechanical components of the module are well within very reasonable limits.

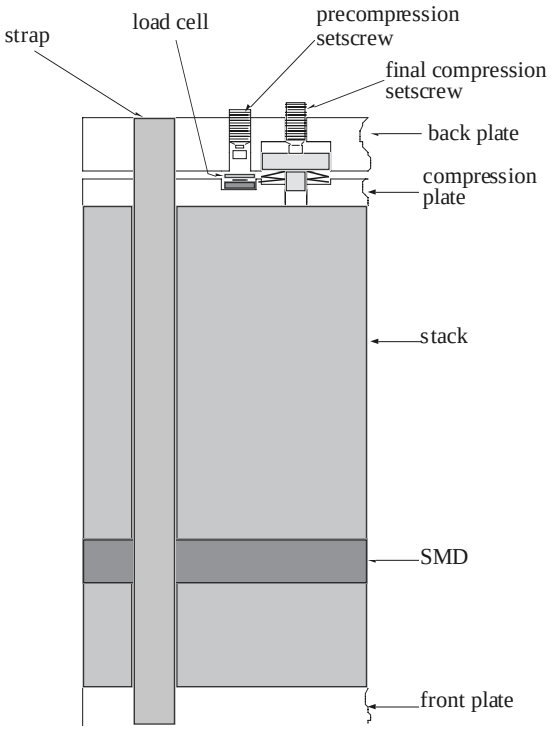


Figure II.2.1-7 Schematic view showing the opening for the load cell and Belleville washers.

The consequences of the non-uniform pressure in the stack have been carefully studied in relation to the light output of the scintillator tiles. An experimental setup was designed in a dark box that allowed us to scan the tiles with cosmic ray muons while under controlled temperature and pressure. The pressure was varied within a range of 0 to 50 psi. Temperatures ranging from 20 to 45 degree C were held constant within 1 degree C during these studies. The test setup is shown in Fig.II.2.1-10. The results of the tests, discussed in detail in section II.3 revealed that the range of pressures encountered in the stack will not impact the calorimeter performance.

The effects of lead creep have been analyzed in order to predict long term structural stability of the EMC modules. The rate of strain of antimonial lead plate (1% Sb), 5 mm thick, under a pressure of 3 kg/cm$^2$ is ~ $5*10^{-6}$ %/h or $2.5*10^{-7}$ mm/h. Thus the shrinkage rate for the stack considering 20 lead plates is ~0.044 mm/year. This rate leads to a very fast decay of pressure in the stack. To slow down this decay, a set of Belleville washers is incorporated in the force loop. These washers are characterized by their nonlinear relationship between load and deflection. The dimensions can be arranged so that a large deflection can be absorbed with very little change in load.

For the load range encountered in the EMC module, a set of certified Rolex Belleville washers XAM-402010, 2 in parallel and 4 in series, has been selected. These washer have been optimized for the 529 lb/screw load. The curve of load vs. deflection for these washers is shown in Fig.II.2.1-11.

The selected washers will control the stability of the module against Pb creep for well over 20 years once assembled. Strict procedures and controls are used in order to insure that the lead has been properly pre-compressed so as to minimize the elasticity of the stack itself at assembly. After stacking, a simple compression protocol is followed to verify that all of the elastic components of the stack are removed. The process of relaxation of the stack can take up to several weeks depending on the waviness of the individual

components used. For this reason, all of the lead sheets are pre-compressed between precision ground steel surfaces before stacking. For the removal of these elastic components, During compression of the stack, the procedure is to raise the pressure slowly in precisely controlled steps and record the rate of pressure decay of the stack as a function of time. Repeated adjustments are made to bring the stack pressure to the rated value. This procedure is continued until the pressure decay becomes ceases at the 1 part per $10^5$ level per day which is the sensitivity of the pressure measurement. At this moment, the load can be transferred from the load cells to the Belleville washers.

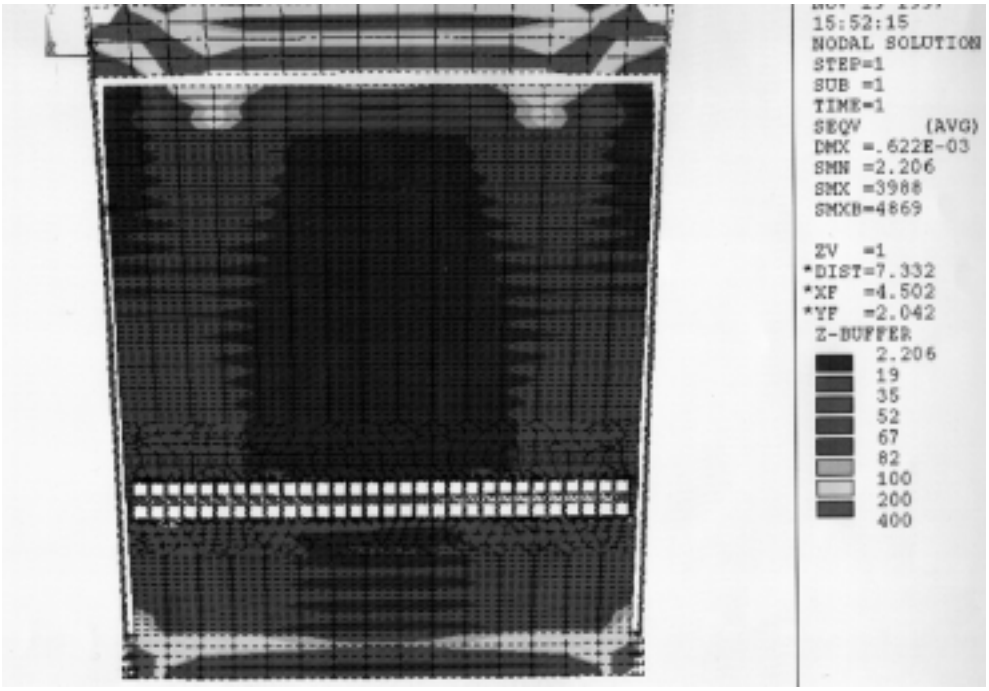


Figure II.2.1.8 Finite element analysis showing stress distribution in the EMC module stack.

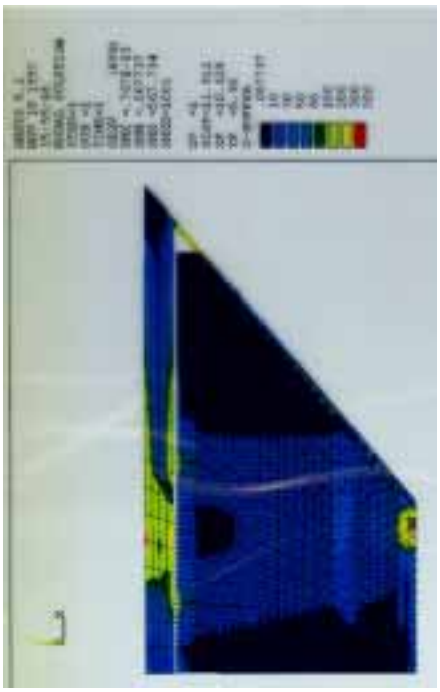

Figure II.2.1-9 Finite element analysis showing stress distribution in the EMC module stack at $\eta = 1.0$

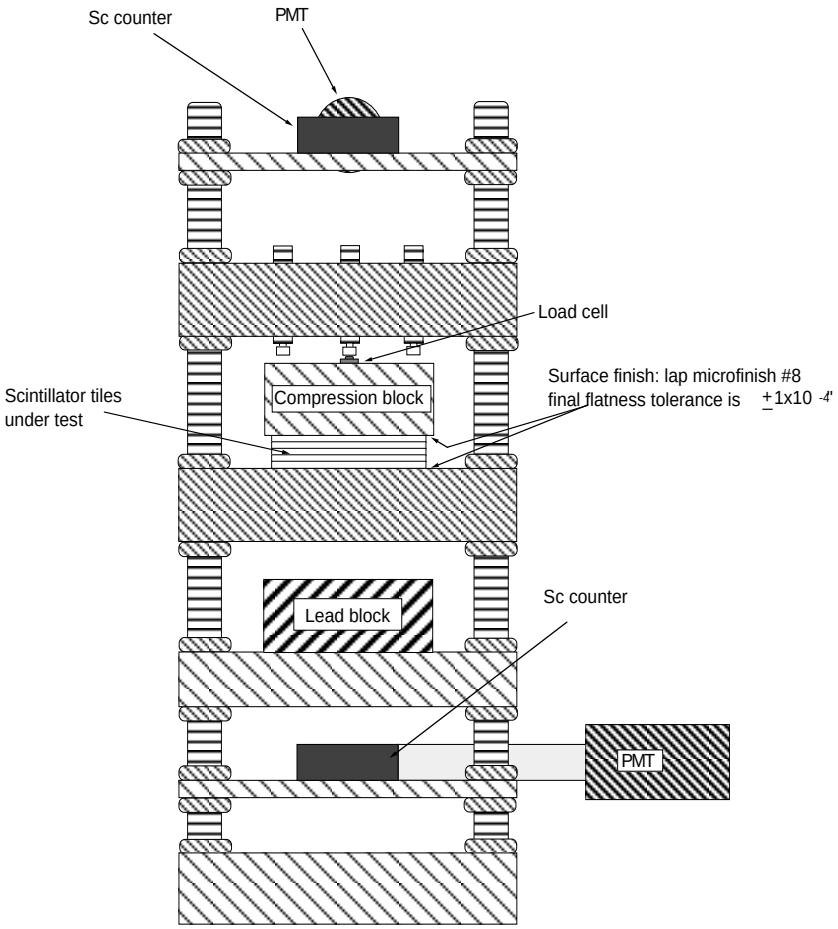


Figure II.2.1-10 Schematic view of the setup used to measure light output vs. pressure of scintillator tiles.

## II.2.2 Module Assembly and Production Plan

During the EMC module prototyping stages at WSU, efforts have been made to scale the facilities and handling equipment for the production requirements of full size EMC modules. These facilities have been upgraded during and have already been utilized in the assembly of a full size module.

For module stacking, a table has been designed that consists of a W12 I beam with 12” flanges weighing 136 lbs/ft. The beam is 12 feet long and rests on a very stable base. The stacking flange has been ground to obtain a final flatness < 0.004” along the

axis of the beam. A set of 10 precision spacers is attached to the top of the beam so that some free space is provided under the module once it is finished to mount straps, install handling arms, install and remove the stacking guides, etc. Two gutters are mounted on either side of the beam for fibers handling.

### II.2.3 Prototyping Activities

Several mechanical and functional prototypes have been made during the design phase of the project. Each of these prototypes has been made using final construction materials. The tests included: studies of mechanical behavior, tests with an AGS beam at BNL, optical tests, cosmic muons tests, long term pressure stability tests, etc. The result of these tests has been used as a feedback loop for the final design of the modules as well as peripheral systems.

The evolution of prototypes at WSU has been as follows. An engineering mechanical prototype was first designed and constructed. The test module design was ~ 80" long but otherwise virtually identical to the existing stack design. The module was used to establish compression protocols and to study the mechanical stability of the stack using a system capable of measuring deflections of the module smaller than 0.001" over 360 degrees of rotation around its center of mass (Fig II.2.3-1). These later tests were important to verify the suitability (coefficient of friction) of the selected construction materials. Using this prototype, tests were conducted to measure the coefficients of static friction, between different components. For this application, a special fixture was designed. This test module was also used to verify, by direct measurement, the calculated pressure distributions within a compressed module. Other studies were related to the pressurizing technique to be used and the measurement of loads in the stack, distribution of pressure in the stack, etc. During all of these various tests, the module was assembled and disassembled approximately 50 times allowing substantial experience to be gained in these procedures.

Fiber routing was also studied with the first mechanical prototype. Studies with both the sigma configuration and the alpha configuration with and without the protection notch were undertaken. Experience gained through these studies, was very important in establishing the final fiber routing scheme.

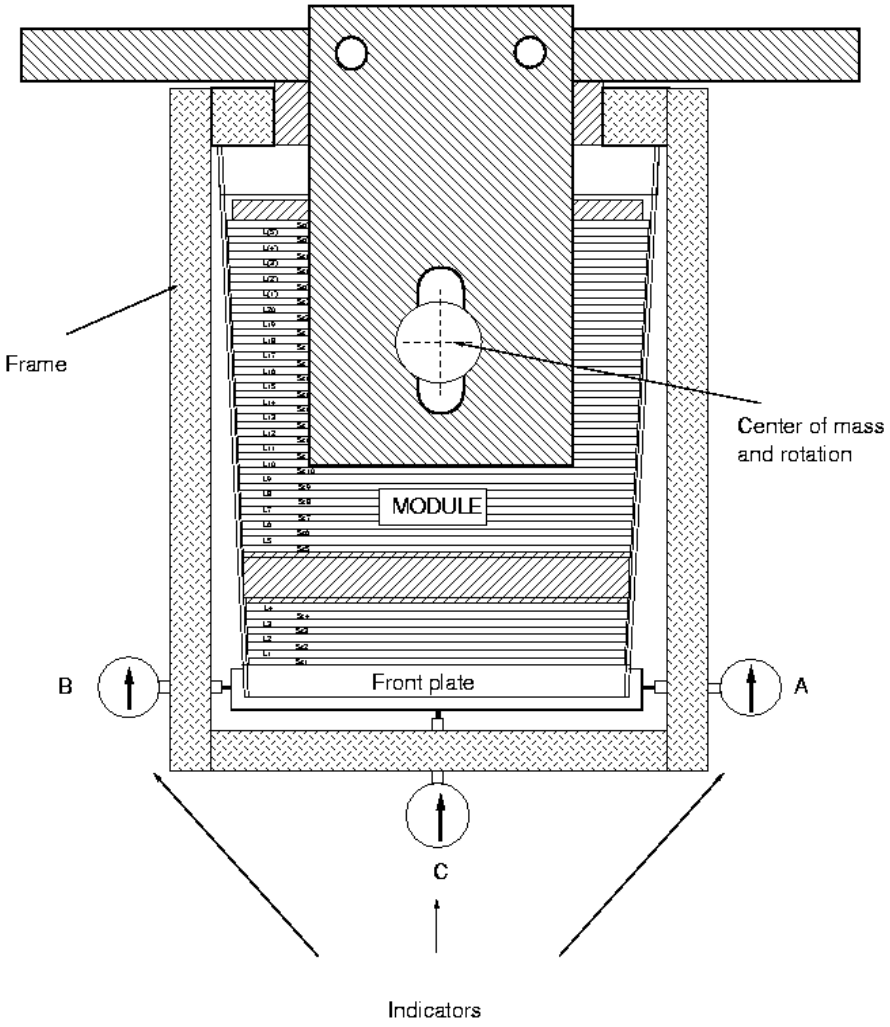


Figure II.2.3-1 Schematic view of the setup used to measure deflections of the module.

The mechanical model was also used to empirically study the thermal expansion characteristics of the stack and verify the analysis used to set some of the assembly tolerances and clearances.

The second prototype was fully instrumented as a detector. The module had eight towers (4 in eta by 2 in phi) assembled from megatiles that spanned the eta=.05 to 0.2 locations in STAR and was geometrically identical to the corresponding section of the STAR module. The module was fitted with a double layer shower maximum detector of a design that will be utilized in the production modules. The module used, however, a number of fiber techniques which have since been abandoned in favor of simpler and more robust techniques. These details of this prototype and its performance in-beam at the AGS are discussed in sections ** (towers) and ** (SMD) below. Pictures of this prototype at different stages of construction are shown in figures II.2.3-2/3/4

The third and possibly the last generation of prototypes is on going now with the construction of a full size EMC module that we plan to test in beam in October. All the

possible improvements suggested by the feedback of the previous prototypes regarding the physics and mechanics have been carried out to obtain a high quality detector.

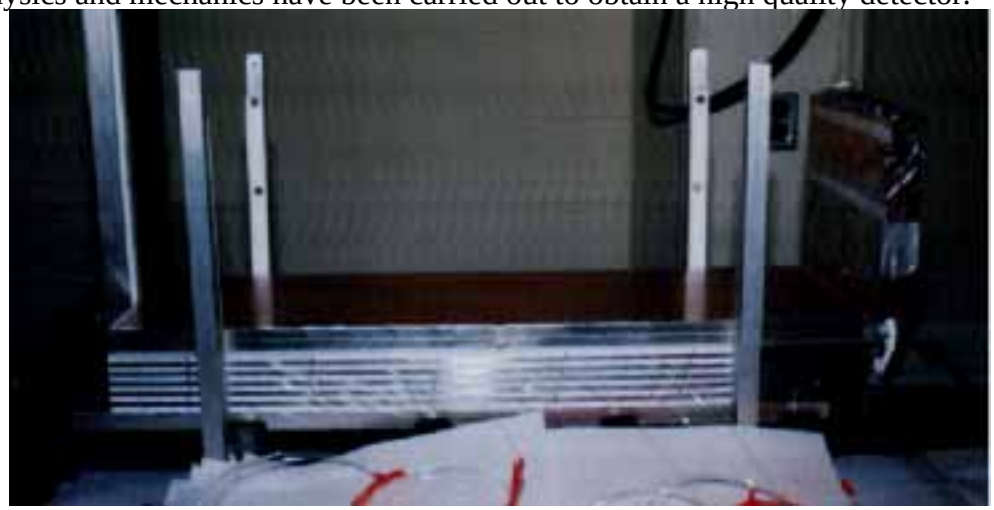

Figure II.2.3-2 Picture showing assembling of the prototype module for the test beam run 1997. The shower maximum detector and its prototype FEE package (on the right) are seen.

Figure II.2.3-3 Picture showing assembling of the prototype module for the test beam run 1997(compression stage).

Figure II.2.3-4 Picture showing the assembled prototype module for the test beam run 1997.(ready to go).

### II.2.4 Quality Assurance Program

Virtually all of the mechanical components of the modules, with the exception of those few better suited for high volume production techniques, are manufactured in house at Wayne State. Regardless of the source, all components are subjected to 100% first part inspection to be followed by critical dimension checks on all parts thereafter. For major parts which will be built over the duration of the project, we will incorporate 100% inspection on a regular basis (e.g. monthly or as appropriate) to guard against gradual erosion of manufacturing standards.

The modules are assembled in precision jigs which provide for the accurate loc a-tion of individual lead and scintillator plates. It is essential to control the positioning of these plates as their location determines the open gap provided for fiber routing between the stack and the tensioning straps. The elements of the jigs which define the positions individual plates must be removed and reinserted for each module. 100% inspection of the assembly jig is thus undertaken before the assembly of a module may begin. Before packing for shipping, the finished modules are subject to an inspection rate of 100% of their critical dimensions.

Traveling documentation will move with each manufactured part to such that an archival record of each of the quality assurance steps is maintained for all the components of a completed module.

As this document is being written we have just completed the assembly of the first full size mechanical prototype and a draft set of assembly procedures now exists based on experience with this first module. This prototype module will shortly be disassembled and reassembled as module-0, the first fully instrumented EMC module (planned for use in the fall 1998 AGS test beam). The draft assembly documentation will be refined and finalized in this process thus archiving assembly procedures to insure uniformity over the duration of the project.

### II.2.5 Safety Matters

All the procedures and material handling at WSU are in compliance with State regulations and OSHA standards.

## II.3 The Optical Design of the EMC Module

### II.3.1 Scintillator Plates Production and Quality Control

The scintillating material used in the Optical system must produce enough light for easy identification of the minimum ionizing particle penetrating the calorimeter and must have good transverse uniformity of the response. Our baseline choice of scintillating material is standard polystyrene-based scintillator system.

**Standard polystyrene-based scintillator system:**
**PS (PSM115) →→→ Primary Dopant (pTP) →→→ Secondary Dopant (POPOP)**

This material has attracted the attention of researchers due to its comparatively high light yield and low cost. Polystyrene (PSM115, the grain size about 3mm) is mixed with finely dispersed scintillation dopants, most commonly used are 0.75%÷2% of paraterphenyl (pTP) and 0.01%÷0.04% of 1,2-bis- (2-(5-phenyloxazolyl))-benzene (POPOP). The choice and concentration of wavelength shifting dyes depends on the specific requirements (direct or WLS read-out) and are under the consumer's control. Figure *II.3.1-1*. shows the typical absorption and emission spectrum of pTP and POPOP [1].

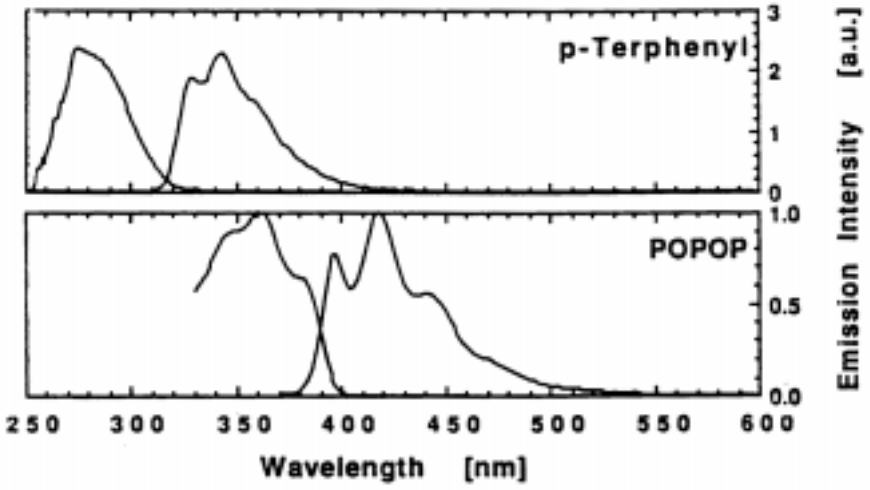


Figure II.3.1-1 Typical absorption and emission spectrums of pTP and POPOP.

The entire EMC contains 5040 megatiles. In order to be practical, the megatile must be machined from 1.6 m long by 0.3 m wide pieces of scintillator. The standard production technique (polymerization between glasses) used to produce scintillator sheets of such sizes are traditionally labor intensive (complicated procedures for glass surfaces preparation, long polymerization time lead to high price and long production time). In order to reduce the cost of scintillator production, the WSU Department of Physics and Astronomy group and collaborators in IHEP (Protvino) adapted extrusion technique that was developed in IHEP [2] for mass production of large scintillation plates required by EMC. The first production batch of scintillation plates, 26 plates (PSM115 + 1%pTP + 0.01%POPOP) with dimensions: 1600 mm x 300 mm x 5 mm were done at UNIPLAST for bench test in 1997. The schematic diagram illustrating the scintillator production and quality control for the EMC is shown in Figure *II.3.1-2.* The scintillating plates are produced in Vladimir – City Company UNIPLAST.

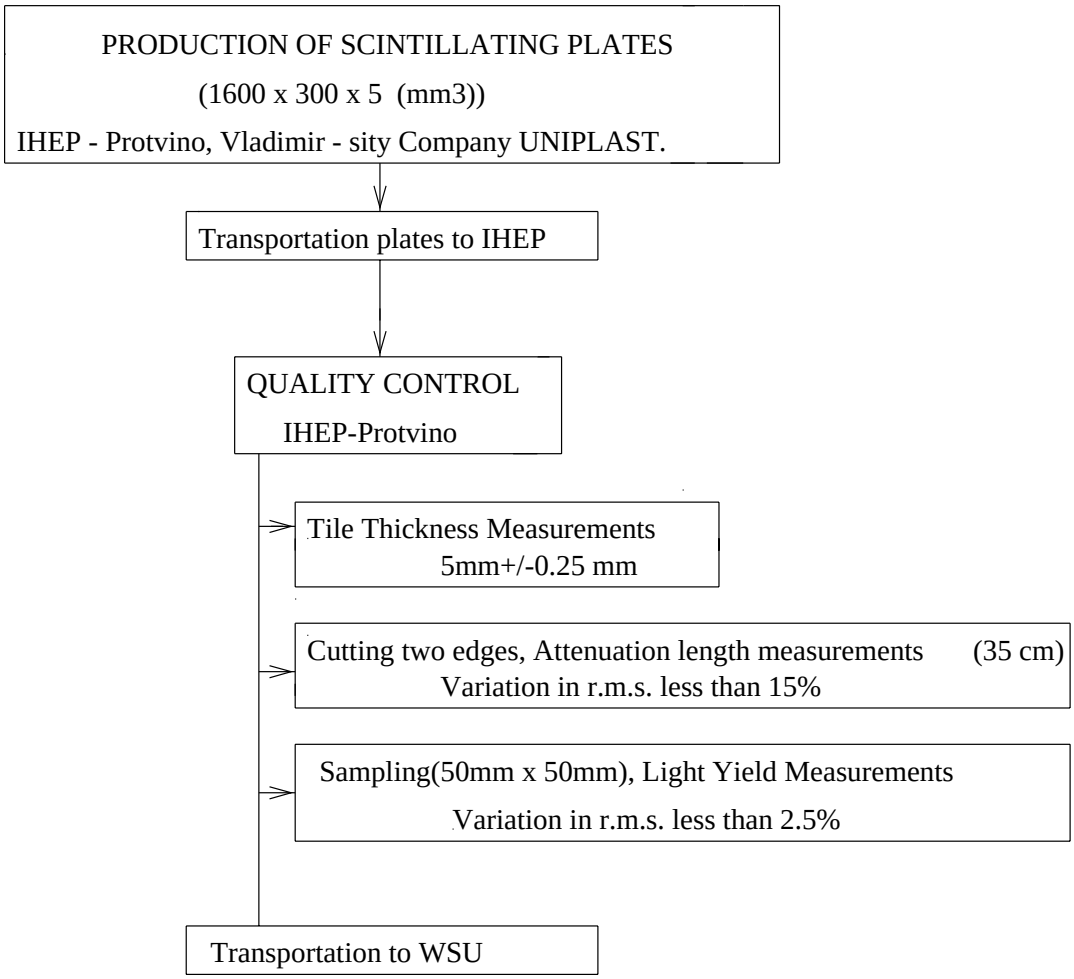


Figure II.3.1-2 Schematic diagram illustrating the scintillator production and quality control scheme for the EMC.

One production lot consists of 55 plates. The plate size is 1600 mm x 300 mm x 5 mm. Several production lots will be sent to IHEP after visual inspection. The program of quality control includes the following:

- plate thickness measurements;
- attenuation length measurements;
- light yield measurements.

The uniformity of response of the tile/fiber system depends on the geometry and the depth of the groove for the fiber, and the uniformity of the light yield of scintillating plates. The light yield of the plates depends on their thickness and the concentration of the wavelength shifting dyes in them. Thus the plate thickness and the dye concentration should be as uniform as possible.

**Tile thickness measurements**

The thickness of all plates will be measured as described below. The special experimental setup with an automatic scanning machine will be used for thickness measurements. The experimental setup is shown in Figure *II.3.1-3.* The scintillating plates will be positioned between two aluminum plates, which have protection cover. The differential transducers will scan tile through slots on the bottom and top aluminum plates. The output current is converted to voltage using a differential amplifier. The voltage values are recorded. The precision of motion is 0.02 mm. We will measure the thickness of a plate at 60 points on 16 lines along X direction. The non-uniform area of 20 mm inside from every edge of the plate will be excluded in this thickness measurement. The number of measured points is 960 in one scintillating plate (total). We require that the thickness of scintillating plates be in the range of $5 \pm 0.250$ mm.

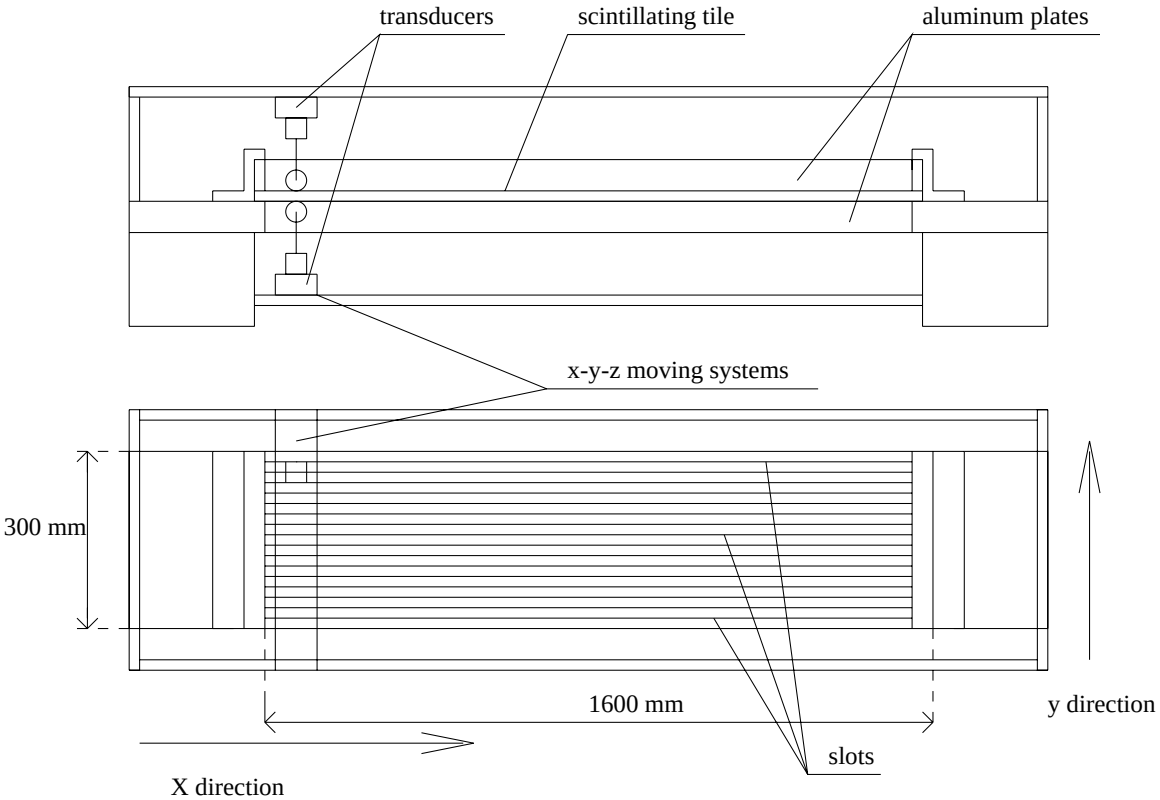


Figure II.3.1-3 Experimental setup for thickness measurements of scintillating plate.

**Attenuation length measurements**

After the thickness measurements, we will cut two edges of scintillating plate and determine the attenuation length of unwrapped plate. A good indication of the uniformity is the attenuation length of the scintillator. As is expected, the longer attenuation length gives the more uniform response. The light output of the scintillator plate as a function of distance from the photomultiplier is usually described by an exponential function. In practice, however, this dependence is notobserded to be exponential for several reasons: the path of the photons is usually longer than the distance between the production point and the photomultiplier due to reflections; light is attenuated by losses in the process of internal reflections. The method of the parameter determination for luminescence optics materials was developed in IHEP[3]. The reflection coefficients of surfaces have to be used in this procedure. The method to calculate absorption length and reflection coefficients uses the measuring amplitude of signals as function of illuminating points coordinates. Figure *II.3.1-4* shows measurements of attenuation length of scintillator sample. The curve drawn in Figure *II.3.1-4* represents calculations using the proposed functional and agrees satisfactorily with the measured values plotted in the same figure. In this method the radioactive source will move along the center of the tile. The source movement will be computer controlled. The systematic uncertainty of this method is typically 3%. We required that the attenuation length should be 35 cm with the rms variation less than 15%.

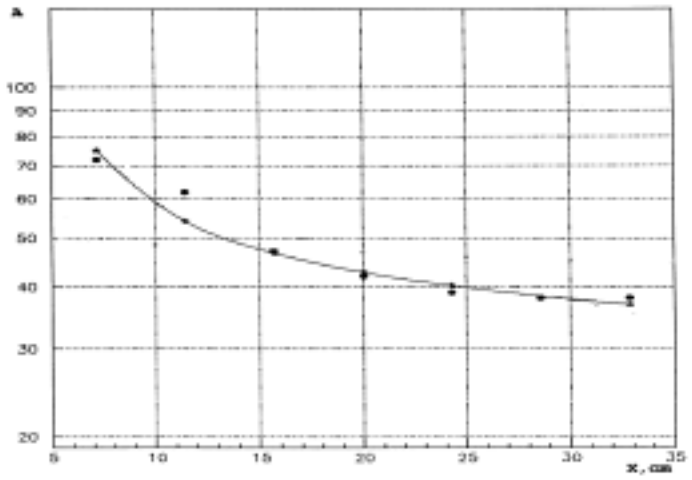


Figure II.3.1-4 Measurements of attenuation length and comparison with calculations.

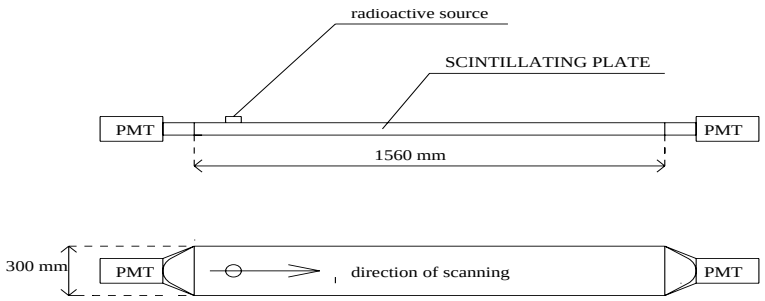


Figure II.3.1-5 shows the scheme of attenuation length measurements.

**Light yield measurements**

We will sample one scintillating block with size 50 mm x 50 mm x 5 mm from one plate of the production lot (one sample from 55 plates). This sample will be used for absolute light yield measurements to check the light variation between production lots. We require that the light yield variation between production lots should be less than 2.5%. Figure *II.3.1-6* shows the scheme of the measurements.

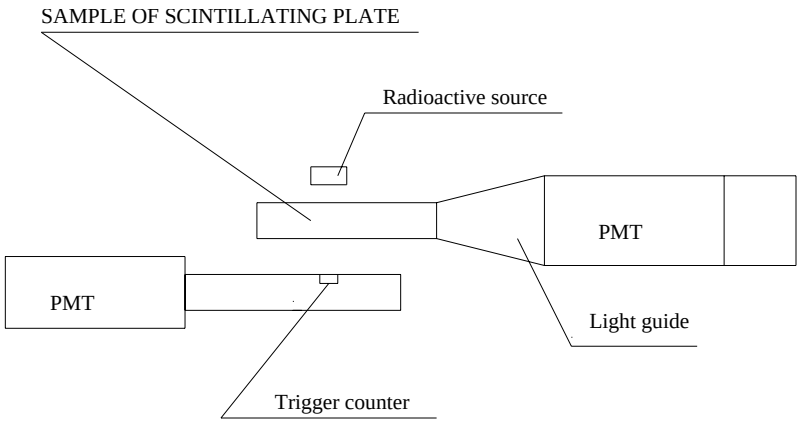


Figure II.3.1-6 Scheme of light yield measurements.

[1]-C.D'Ambrosio et al., CERN/PPE 90-96
[2] - T.V. Alimova et al., Preprint IHEP 86-35, Protvino, 1986.
[3] - V.S.Datsko, N.A. Datsko, Preprint IHEP 95-113, Protvino, 1995.

## II.3.2 Megatile Design, Fabrication, and Quality Control

### II.3.2.1 Megatile Design

As discussed in section II.1, the desire to have a calorimeter with segmentation that is not only projective in $\eta$ and $\phi$, but constant in $\Delta\eta$, leads to scintillator tile sizes that are mechanically different for not only for each tower, but also for each layer. With 40 towers per module, and 21 layers of scintillator per tower, there are a total of 420 different sized tiles in the calorimeter, with 2 tiles of each size. Due to the large number of different sized tiles needed, techniques such as injection molding become impractical because of the cost of the molds. The technology chosen for the construction of the STAR EMC is that of megatile production as used in the CDF Endplug upgrade project[i]. In this process, a single large sheet of scintillator is machined by a Computer Numerically Controlled (CNC) router into a large number of separate tiles. With the use of computer control, the tiles can easily be made to be different sizes using a single set of production tooling. The machining will be carried out in dedicated facilities currently being setup at WSU. The design of these facilities, and the scintillator machining techniques that will be employed, have benefited greatly by the large amount of prior experience gained at FNAL during the CDF Endplug upgrade project[ii]. The facilities and the stages involved in tile production are detailed in the following section.

II.3.2.2 Megatile Fabrication and Production Facilities

The scintillator material is obtained from UNIPLAST in the form of sheets 1.6m long, 0.3m wide, and 5mm thick. Two such sheets are needed for each scintillator layer, and hence the megatiles are roughly half the length of a module. The scintillator sheets will be machined into megatiles on a dedicated, flat bed, Technoisel 4' $\times$ 8' CNC controlled routing machine. The routing machine will be equipped with a vacuum chuck to secure the scintillator during machining. Two identical tiles will be cut at the same time by using two high-speed machine heads. Each head will be equipped with vacuum dust collection facilities and telephoto TV cameras to monitor the machining process. The FNAL group has found that the key requirements for successfully machining scintillator are to maintain low temperature and low humidity, and to critically control the material feed rates depending upon the environmental conditions. The scintillator is kept cold by high pressure cold air guns, and the entire machine will be situated in a climate-controlled room. Based upon prior experience machining scintillator at both FNAL and WSU, two such machines will be needed to keep up with a maximum production rate of 35 modules per year.

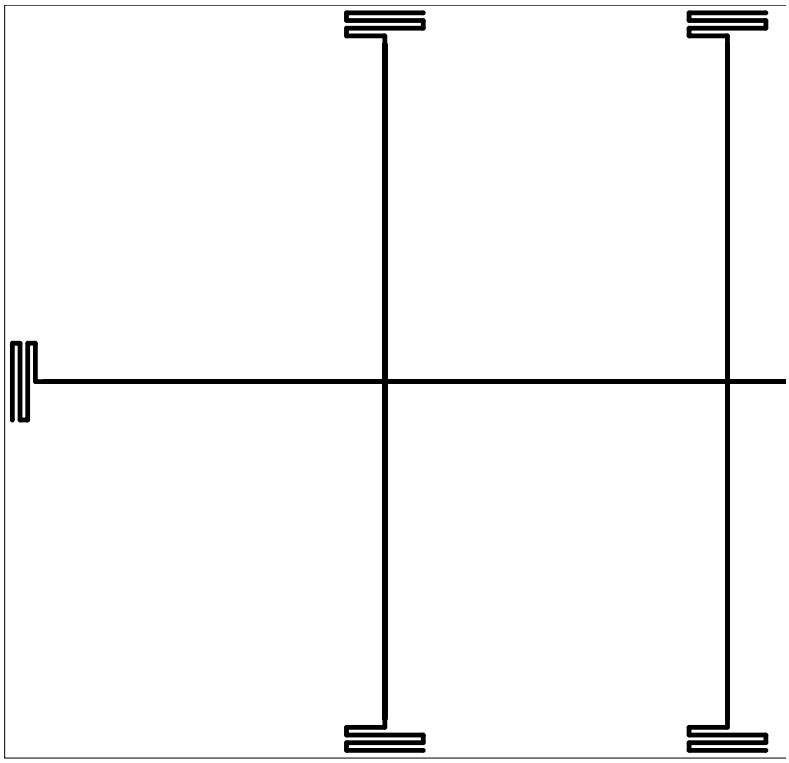

Figure II.3.2-1. Schematic drawing showing the end four towers of a megatile after the separation grooves and epoxy storage labyrinths have been machined.

The first stage in tile machining after the scintillator blank is qualified is to machine the grooves that will later be filled with reflective epoxy to optically isolate the individual tiles from their neighbors. These separation grooves are shown for part of a megatile in figure II.3.2-1. The grooves are machined through all but 0.25mm of scintillator, as shown in the tile cross-section in figure II.3.2-2, leaving the complete megatile physically connected through a thin bridge of scintillator. The scintillator tile is deliberately over-sized so as to leave a border around the tile. This border serves two purposes. Firstly, it provides mechanical strength for the tile prior to filling the grooves with epoxy, though careful handling of the tiles is still necessary at this stage to prevent irreparable damage. Secondly, it allows epoxy storage labyrinths to be machined at the end of each groove as seen in figure II.3.2-1. The labyrinths are described in more detail below.

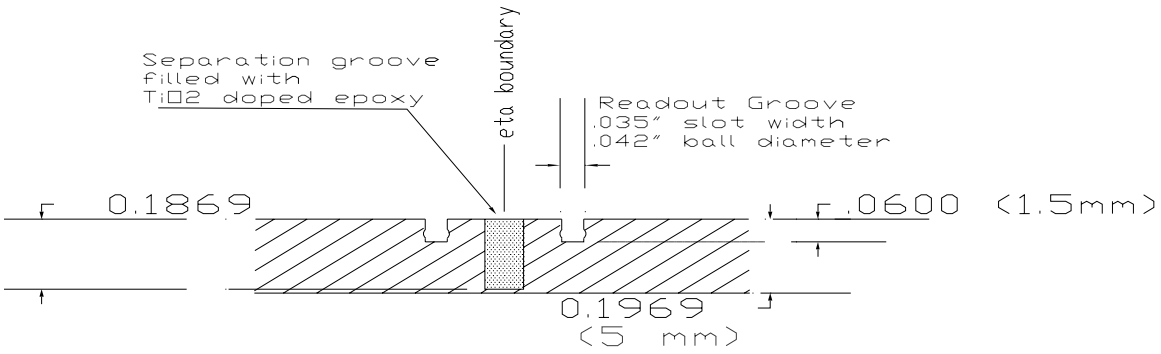


Figure II.3.2-2. Schematic diagram of a cross-section through a tile, showing the separation groove and the two ball grooves which contain the WLS fibers.

After machining the separation grooves, the next step involves injecting $TiO_2$ loaded epoxy resin into the grooves. The techniques used for this operation are identical to those developed during the CDF Endplug project[iii]. The megatiles are first inspected for flaws in the separation grooves that might complicate the process of epoxy injection. Next the top of each groove is covered with Kapton tape to form a closed tunnel into which the epoxy can be injected. Air release holes are added at the far end of the grooves, and epoxy is injected using an automated fluid injection system filling the whole groove and the labyrinths. The tiles are then cured at room temperature. The epoxy has the property that it shrinks upon curing, so the purpose of the labyrinths is to provide a reservoir of epoxy that could be drawn into the body of the tile during curing. This reduces the need to touch up the tile at a later point, and since the labyrinths are beyond the tiles fiducial boundary, they can be safely removed during the next step in the machining process. After curing, the Kapton tape is removed, and any imperfections in the epoxy such as small air bubbles are carefully touched up.

The next stage in manufacture involves returning the now much more robust tile back to the router, where the fiber readout grooves are now machined. After detailed study of the optical properties of various different configurations, the EMC collaboration has decided upon $\sigma$-grooves. These $\sigma$-grooves are machined into the tile to a depth of 1.5mm and then the tile border is machined away to leave the finished tile of which part is shown in figure II.3.2-3. Since the fibers must be routed along the sides of the modules exit notches are cut at the center of each tile. These allow the fibers to exit the tiles parallel to the module's surface.

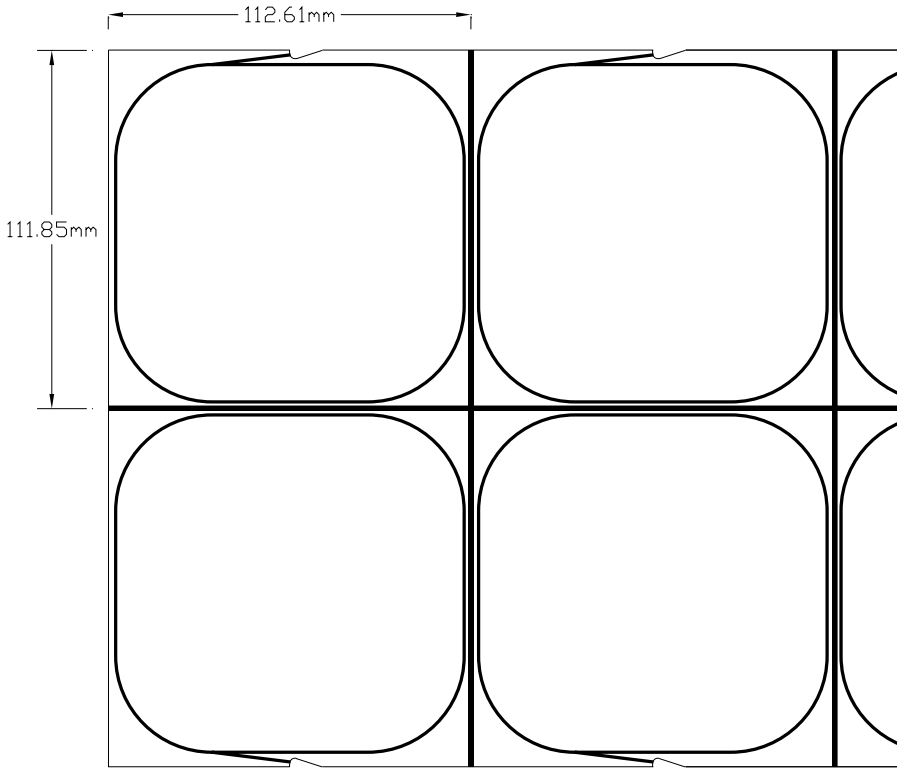


Figure II.3.2-3. Schematic drawing showing the end four tiles of a megatile after fabrication.

The final stage in megatile fabrication is to apply a black ink line to the underside of the tile along the separation grooves. Since the separation grooves do not go all the way through the scintillator, and there is 0.25mm bridge of scintillator left connecting the individual tiles, there is the possibility of optical cross talk. The CDF group[iv] found that this cross talk could be significantly reduced by the application of ink, since this absorbs any reflection off the back surface of the scintillator. The tile is now complete, and passes onto quality control described in the next section. Figure II.3.2-4 shows a photograph of a completed tile ready for assembly in the small prototype, which was tested in BNL in 1997.

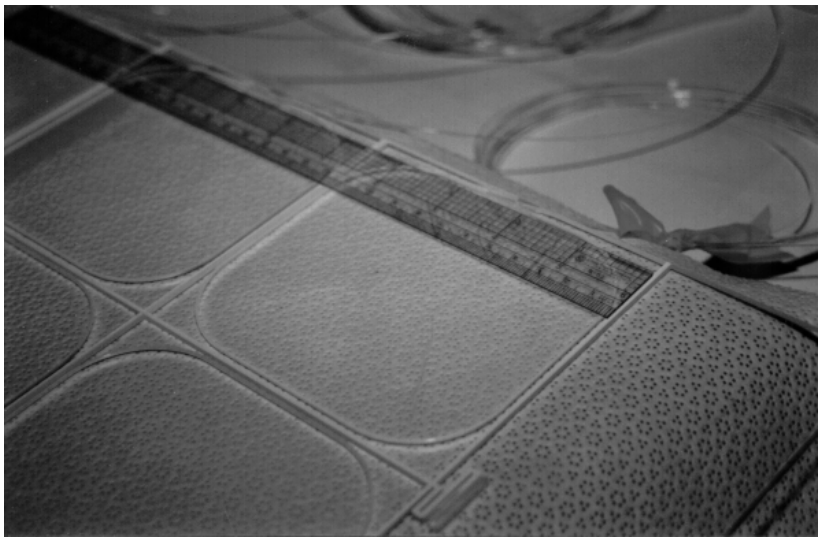

Figure II.3.2-4. Photograph of a completed megatile ready for installation into the small prototype. As this is a prototype tile, the tile border at each end of the tile has not been removed, and the epoxy storage labyrinth is clearly visible.

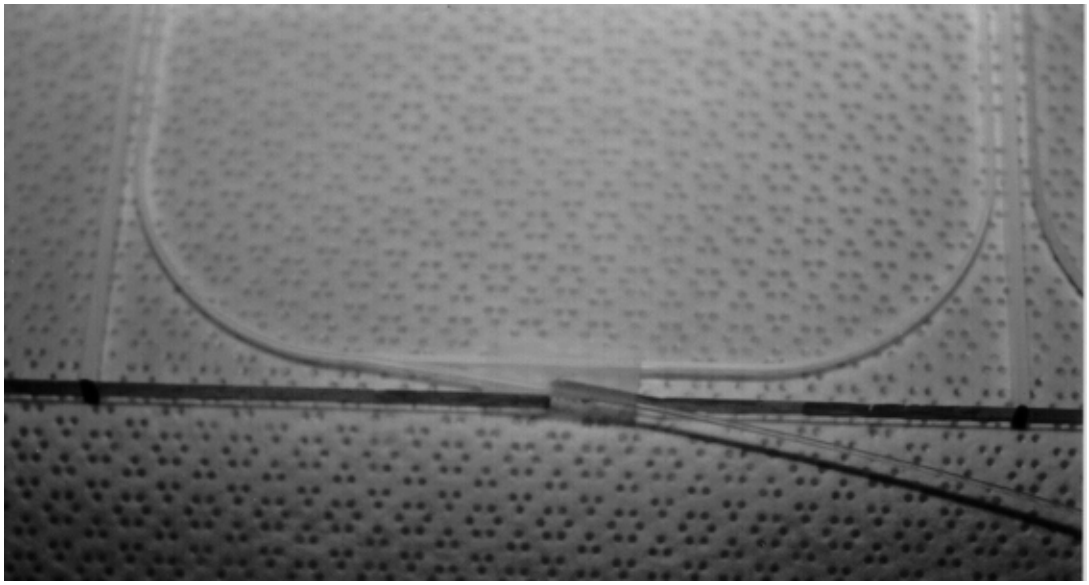

Figure II.3.2-5. Photograph showing a close-up of one of the tiles of the small prototype. Clearly visible are the epoxy filled separation grooves, the readout groove together with its WLS fiber, and the notch to allow the fiber to exit the tile along the side of the module.

### II.3.2.3 Megatile Quality Control

Quality control for the megatile happens at several stages during their manufacture. Because the scintillator is checked for its optical properties by the IHEP group prior

to shipping it to WSU, all the quality control checks performed during manufacture are mainly physical inspections. After the tile is completed it is moved to the testing laboratory. Here, 100% of all tiles will be measured by scanning them with a radioactive source modulated with a lead chopper. The source will be positioned at the center of each tile, and the light generated by the source is readout via a wavelength shifting fiber and PMT. The current from the base is used to feed a lock-in amplifier that is in turn logged by a personal computer. Data will be collected for each tile in the calorimeter, and megatiles failing the 10% RMS requirement will be reworked if possible or failing that rejected.

### II.3.3 Fiber Cable Fabrication and Quality Control

#### II.3.3.A Introduction

The EMC Modules are designed to have optical fibers running from the scintillator tiles through the backleg iron of the magnet to PMTs residing in boxes located on the backlegs. For mechanical and optical transmission efficiency reasons the fibers are broken up into three sections (see Figure II.3.3-1). The first section is composed of wavelength shifting fiber that runs from the tiles to the top of the module. The second section runs from the module through the backleg to the boxes housing the PMTs. The third section runs from the outside of the boxes to the PMTs.

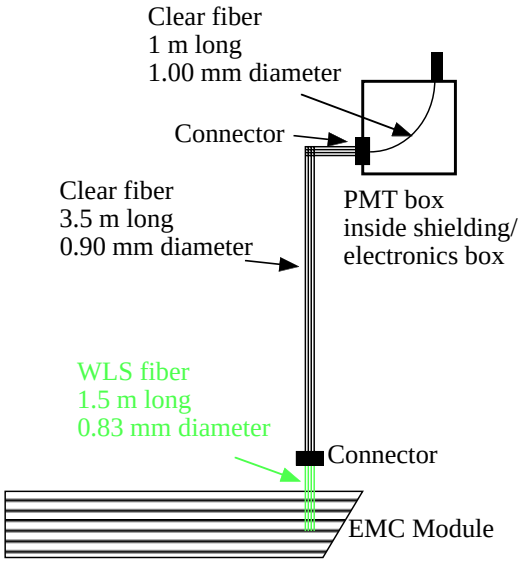


Figure II.3.3-1. Schematic drawing of the fiber read-out system.

#### II.3.3.B Design

The design, construction and fabrication of the EMC fiber bundles are patterned on the Michigan State University High Energy Physics (MSU-HEP) program for making fibers for CDF. Briefly, that experiment called for cable bundles of ten fibers but otherwise has a similar design. The fabrication facilities, personnel, etc. still exist at MSU and are partially available to the EMC project. Given the cost and time saving benefits, a decision was made to modify the EMC fiber scheme to the 10 fiber bundles and use the MSU facilities.

Each tower of the EMC has 21 scintillator layers each requiring an optical fiber. Two preshower layers, the first two layers of the calorimeter, will have two fibers each. The 23 fibers will be grouped into 2 cables with 10 fibers each and the remaining 3 will share a partial bundle with a neighboring tower. To maximize the light transfer though each of the 3 cable sections between the tiles and the PMTs, the fibers in each subsequent cable will be larger in diameter than those of the preceding cable. The diameters are 0.83, 0.9, and 1.00 mm. This scheme leads to 8 cable styles. The 0.83mm WLS fiber will have two styles of 10 fibers each with the fiber lengths cut to fit the appropriate depth in the tower. The third cable will share fibers with the neighboring tower. The 0.93mm fibers running through the backleg will all have the same length but one cable style will have 10 fibers and the second six. The 1.0mm fibers in the PMT boxes will also have three styles to match the various lengths needed to reach the PMTs as well as to match the one cable with six fibers.

| Style | 10 fibers top | 10 fibers middle | 6 fibers bottom |
|---|---|---|---|
| 0.83mm WLS | 4800 each | 4800 each | 2400 each |
| 0.93mm Clear | 9600 each | n.a. | 2400 each |
| 1.0mm Clear | 4800 each | 4800 each | 2400 each |

**II.3.3.C Fabrication**

The steps required to fabricate the cables are well understood by the MSU-HEP group. The general steps are as follows:

1. Prepare fibers
2. Prepare connectors
3. Epoxy fibers into connectors
4. Polish connector ends
5. Clean cables
6. Measure light transmission
7. Store in shipping boxes.

The cable fabrication facilities at MSU-HEP are in a dedicated room with “stations” for the aforementioned steps. Each of these stations has fixtures, jigs, etc, designed to hold multiple connectors and or fibers for mass production. Given the volume of cables that have to be made it is expected that facilities at NSCL will be built to compliment those of the HEP. Following is a list of the major stations.

1. Cutting
2. Gluing
3. Diamond Polishing Machine
4. Testing

Table 1 shows the detailed steps and the required time. These times are actual times based on previously constructed cables made by the HEP group. For the EMC additional steps are required to mirror the ends of the fibers that go to the tiles. This is done with a sputtering technique designed by and done at Fermilab. In addition, the sheathing used by the HEP group is not light tight and additional steps will be required to meet the EMC's requirement of the cables being light tight.

It is expected that the cables will be made over an approximately three to five year period. Given the 5000 man-days of labor required, 7 people working full time for three years is needed. Because student labor will be used and the number of hours a student can work is limited, it is expected that a crew of 14 or so people will actually be employed. MSU-EMC group, with technical support from the MSU-HEP group, will do the supervising and training. The module construction timetable and the shutdown periods of the STAR detector will dictate the actual fiber construction schedule.

| Task | Description | Est. time (min./cable) |
|---|---|---|
| 1 | Inspect cables for defects | 2 |
| 2 | Cut cables to length | 1 |
| 3 | Prepare and clean connectors | 2 |
| 4 | Prepare and attach labels to the cable | 2 |
| 5 | Trim cable ends | 1 |
| 6 | Hang the cable at the gluing station | 1 |
| 7 | Strip the covering from the cable ends | 5 |
| 8 | Prepare and attach the strain relief tape | 3 |
| 9 | Setup connectors in the gluing stand | 1 |
| 10 | Trim the covering and strain relief | 2 |
| 11 | Insert cable ends into the connectors and clips | 2 |
| 12 | Glue the cables into connectors | 5 |
| 13 | Transfer cables to carrying trays | 1 |
| 14 | Polish the connector ends | 8 |
| 15 | Remove excess glue and clean the cable ends | 2 |
| 16 | Attach the connector clips | 1 |
| 17 | Measure light transmission through cable | 5 |
| 18 | Analyze test results, examine failures | 3 |
| 19 | Make the storage/shipping boxes | 1 |
| 20 | Store/ship cables | 2 |
| 21 | Cable repairs, remakes (avg.) | 4 |
| 22 | Supervision, training, documentation*, etc. | 5 |
| 23 | Housecleaning, maintenance, etc. | 5 |
| TOTAL | | 64 |

(* Many tasks require an entry on a traveler sheet documenting cable#, date and person completing the task.)

Table II.3.3.C.

### II.3.3.D Quality Control

The EMC quality control will be similar to that of the MSU-HEP project. However, the final variations are still under discussion. In addition to visual inspection of the fibers before construction of the cables, the cables are checked after gluing and polishing. The MSU-HEP method for the clear fiber is:

> "The cables are tested by inserting each cable into an optical path consisting of a calibrated source and a photodiode detector. One source and one photodiode are used for each of the 10 fibers in the cable. The sources consisted of lengths of the same WLS fiber as used on the calorimeter, illuminated with a fluorescent UV bulb. The currents from the photodiodes are measured using a pico-ampmeter readout via GPIB bus to a PC. A low impedance multiple switch controlled by the PC is used to select the photodiode. Since we were interested primarily in the variation of light transmission from scintillators in the same readout cell, we tabulated the corresponding rms variation using fibers in the same position from a group of cables. For example, the rms variation from the average for fiber number 3 in set of similar length cables would be tabulated. Cables having any fiber with deviation greater than 10% from average would be examined for problems and those with deviation greater than 15% would be re-made. The rms variation/average transmission for the whole set of cables was about 2.5%."

In the case of the PMT box cables this concept will have to be modified to account for the varying lengths of fiber.

This method, however, will not work for the WLS fibers that are aluminized on one end. An alternate proposal is being made to measure these fibers. This proposal is designed after a method used at FERMI lab where the fibers are irradiated with UV light passing over the length of the fiber with the output continuously measured and recorded via a photodiode response.

### II.3.4 Scintillator and Megatile Performance Studies

The tile/fiber sampling technique is chosen for our calorimeter design. This technique uses scintillator tiles to sample the electromagnetic shower. Wave-shifting fiber (WLS) embedded in the scintillating tile traps the scintillator light and clear fiber connected to the WLS fiber carries the light to photomultiplier. The EMC requires a total of 90,800 scintillating tiles. The cost per tile is an important parameter in the choice of the tile material. This issue has led us to the choice of PS extrusion scintillator for EMC. The most important problems of optical system on the base of PS extrusion scintillator were to achieve and maintain a uniform, minimum light yield so that the resolution of EMC is not compromised by a lack of photostatistics. PS scintillator with the extrusion technique has been proved to have inferior light yields compared to cast scintillator. However, requiring light yield from tile more than 2 photoelectron/MIP, it is possible to use this material, but at the expense of optimization of all components of optical system. This optimization include the following:

1. studies of the dependence of the light output of the tiles on the pattern of fiber groove;
2. selections in the optical read-out chains, which include choice of material for other parts of the optical system (WLS and clear fibers, optical connectors);
3. detailed studies for identification the requirements for components of optical system;
4. studies of possible causes, which can change of the absolute light yield and uniformity response of the scintillator tile.

As a result, we found the pattern of fiber groove in tile and configuration of optical system, which produced light yield more than 2 photoelectrons/MIP and uniformity response over the surface of tile better than 3% rms. We have chosen this configuration of optical system to go into production for the Electromagnetic Calorimeter of STAR. Results optimizations of optical system are discussed in this Chapter.

### II.3.4.1 Absolute light yield measurements of different tile/fiber assemblies

In order to optimized optical system we study the dependence of the light output of the tiles on the pattern of fiber groove and type of read-out WLS fibers. The light from tile re-emitted by the WLS fiber is then transported directly by the WLS fiber or by the clear fiber thermally fused to a WLS fiber to the phototube located on the distance about 3 m from scintillating tile. We have compared the absolute light yield of eleven different tile/fiber system using $\alpha$- and $\sigma$-grooves. Extrusion PS scintillator of 5 mm thickness were used as a standard. Some date were taken for Bicron BC404A scintillator as a comparison.

Figure *II.3.4.1-1* shows the principal scheme of read-out chan for tile with $\alpha$ - and $\sigma$-groove pattern of fiber groove.

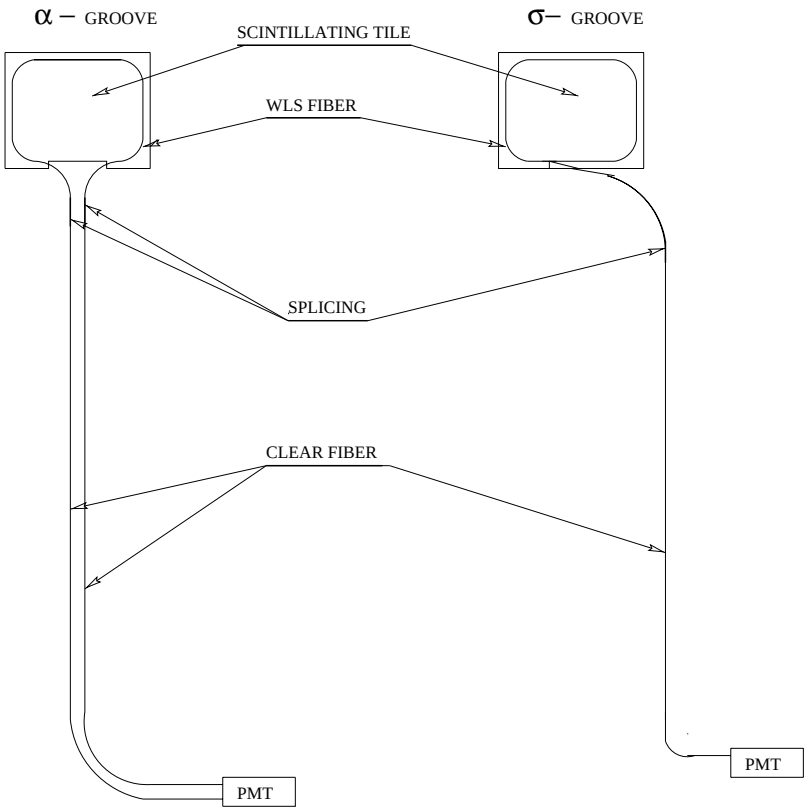

Figure II.3.4.1-1 Principal scheme of read-out chain for tiles with α - and σ - pattern of fiber groove.

Figure *II.3.4.1-2* shows a schematic drawing of geometry of the test setup[1], which has been designed and constructed at WSU during 1996. This experimental setup is a part of a quality control program of the calorimeter tile production, and is designed to monitor the absolute light yield and light yield variation of individual tiles.

The apparatus consisted of three independent parts: two fixed frames for mounting trigger counters and a radioactive source, together with a movable table used for mounting the scintillating tile currently under test and the phototubes (PMT). All parts of the setup were mounted in a light isolated box. The temperature inside box was continuously monitored. The tile under test was mounted on a table which is moved by stepping motors controlled by a personal computer, thus allowing the light output of tile (or megatile) to be scanned transversely as a function of position. The range of motion is 200 mm in both the X- and Y- directions. The precision of motion is 0.25 mm. The trigger counters are mounted on the fixed frame located above the movable table. Each trigger counter consisted of a 2 mm x 2 mm Bicron BCF-12 scintillator coupled to an Hamamatsu RC4044 PMT. By using two trigger counters in coincidence we eliminated non-local and non-penetrating backgrounds such as gamma rays and low energy electrons.

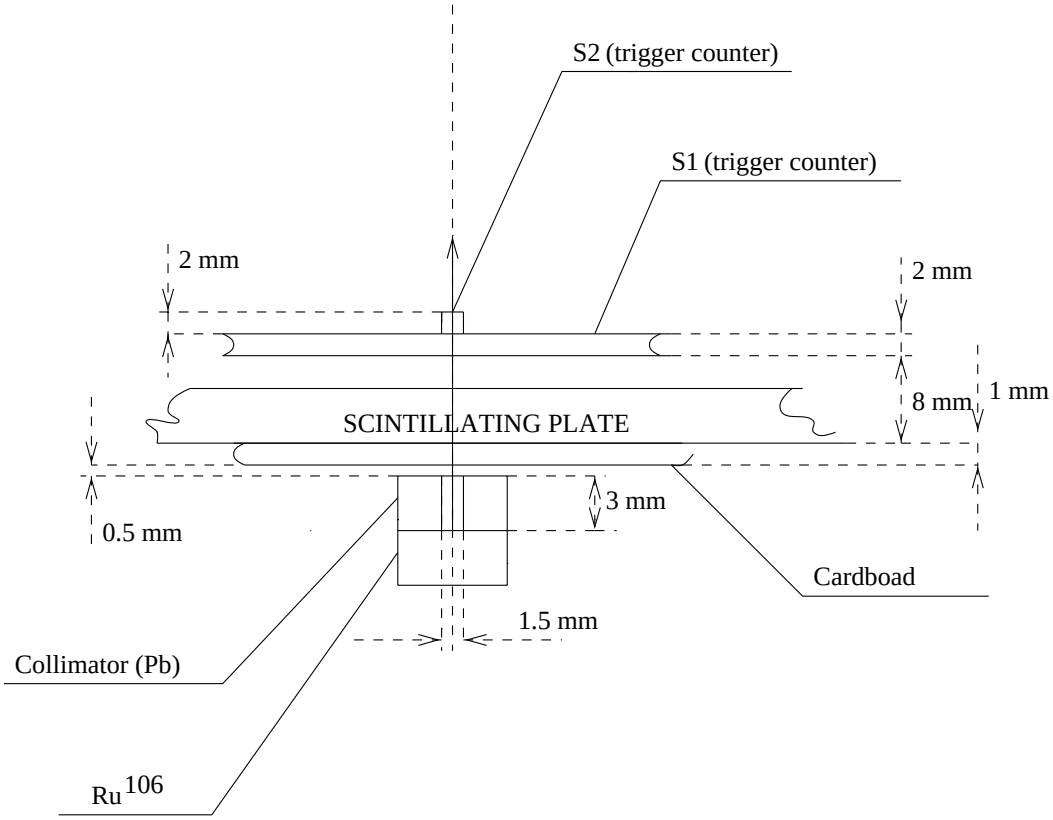


Figure II.3.4.1-2 Schematic drawing of geometry of the test setup.

The scintillator tile under test was excited by a Ru(106) 3 MeV β-ray source of 8 mm in diameter, which mounted on the fixed frame below the movable table. At this energy the electrons are approximately minimum ionizing in the first several mm of plastic scintillator. Their range is great enough to penetrate: 1mm of cardboard, the 5 mm thick scintillator tile under test, and a 2 mm thick trigger scintillator, to finally deposit a signal in the last 2 mm trigger scintillator. Multiple scattering in the scintillator is not too large considering our spatial resolution of 2 mm. Light from file/fiber assembly was detected by the PMT (Hamamatsu R580-17) currently under test. The signal from the PMT is digitized by LeCroy 2249A CAMAC ADC module with a maximum resolution of –0.25pC/channel and recorded by personal computer. The single photoelectron peak for the PMT under test had been obtained using the tile/fiber system by reducing the detection efficiency to approximately 0.1 so that the contribution of 2 photoelectrons was made negligibly small [2]. An LED based flasher system is also used for calibration purposes. The light from a blue LNG992CF9 LED is transported to the PMT via a green Bicron BCF91A WLS optical fiber of 1 mm in diameter. A comparison of the results obtained between the PMT calibration using the tile/fiber assembly and LED system has not shown significant differences. We estimated the light yield from a tile/fiber system in terms of an average number of photoelectrons produced by the photoelectric affect on the PMT photcathode [3]. For the uncertainty in the number of photoelectrons we evaluated

effect of the reproducibility of measurements due connection fiber to PMT. This uncertainty is not more than 10%.

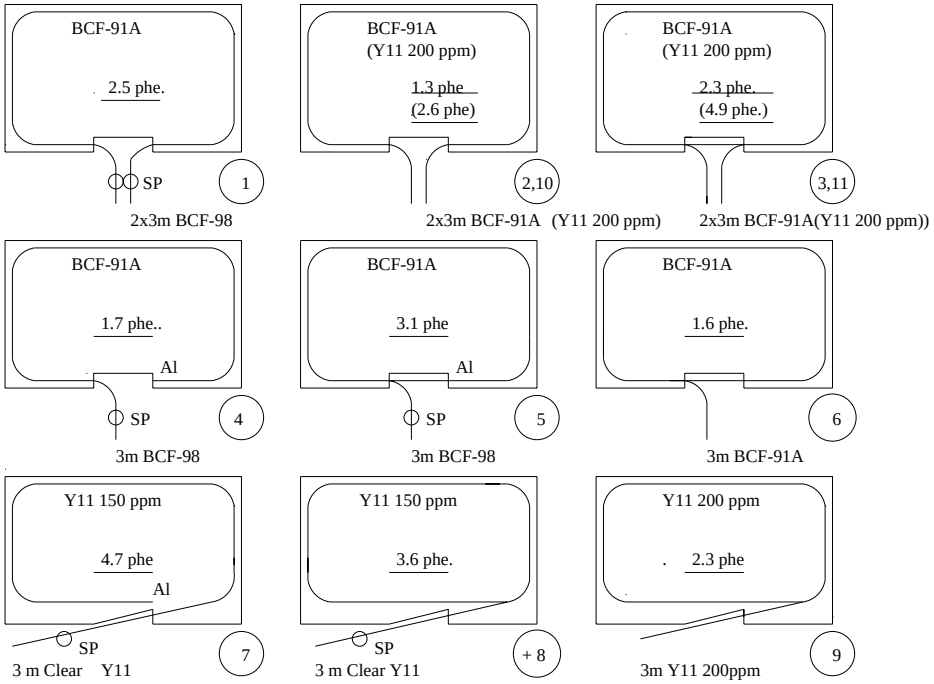


(Bicron)BCF-91A - green WLS fiber.

(Bicron)BCF-98 - clear fiber.

(Kuraray)Y11 150 ppm(200 ppm) - multiclad S-type green WLS fiber (ppm - the numbers in the parentheses . correspondent to number of parts per million by weight of fluorescent dye in the fiber core.

(Kuraray)Clear Y11 - multiclad clear fiber.

Al - aluminum mirroring.

SP - splicing.

Figure II.3.4.1-3 Schematic diagram of different optical schemes

The read-out patterns differed in the number of fibers laid in the groove (one or two loops of WLS fibers) and one ($\sigma$-groove) or two ($\alpha$-groove) fibers connected to a PMT. For schemes 1-6,10,11 we have used tile with dimensions: 125 mm x 132 mm x 5 mm and tile with dimensions: 125 mm x 190 mm x 5 mm for schemes 7-9 (biggest tile sizes). WSU Department of Physics and Astronomy group fabricates the sample tiles. Many aspects of the scintillator tile design, such as the depth of the read-out groove, the groove shape, the groove location with respect to the tile borders are based on research done by the CDF and SDC group[4, 5, 6, 7]. A peripheral groove was machined in the tiles with a dental drill bit at high speed and as close to the edge as possibly.

The groove has rectangle shape with width 1.25 mm. The distance of the groove from tile edge was 1.5 mm. The groove makes a turn by 90 degree at the tile cones at radius of 30 mm. As shown by the CDF and SDC studies, this radius of 30 mm is optimal. At a large radius the response near the tile corner outside the fiber groove was measured to drop substantially. We chose the groove depth of 2 mm, which is optimal for 5-mm thick scintillator. Each sample tile has narrow notch or slot for fiber exit. The non-polished tile edges are painted white with Bicron BC620 reflective paint[8]. White bond paper is used

on both sides of the tile as reflector[9]. The main results of these measurements indicate that:

- all optical schemes ( exception: 2, 4, 6) met design criteria that the light yield should be more than 2p.e./MIP;
- the highest light yield corresponds to the α-groove with two loops of WLS fibers (scheme 11) and σ-groove with mirrored multiclad WLS fiber spliced to clear multiclad fiber;
- the light yield of the tile (σ-or α- groove) with two loops of WLS fiber embedded in one groove is 1.8 times higher than the light yield of the tile with one loop ( schemes: 2,10 – 3,11 and 4-5);
- comparison of the single ended aluminized σ-groove read-out (scheme 4) vs. α-groove read-out (scheme 1) have shown that 1.47 times the light is recorded with the latter;
- the use of a Kuraray multiclad Y11 WLS fiber spliced to a multi clad Kuraray clear fiber increases the light yield in 2.8 times, compared for Bicron singleclad WLS fiber spliced to single-clad Bicron clear fiber (schemes 4,7);
- comparative light yield measurements for the Bicron 404A scintillator and PS extrusion scintillator (PSM-115+1%pTP+0.01%POPOP) showed that the Bicron 404A scintillator yields a factor of 1.6 (scheme:7);
- test comparing the light collection efficiency from PS scintillator tiles with both Bicron and Kuraray multiclad Y11 (200) WLS fiber show that the Kuraray improves the light yield by a factor of 1.6.

### II.3.4.2 Study the uniformity of the response

The uniformity of the response of the tile/fiber assemblies has been measured using the ANL and WSU experimental setups with collimated Ru (106) source. Figure *II.3.4.2-1* shows the result of this measurement for PS scintillator with α-groove.

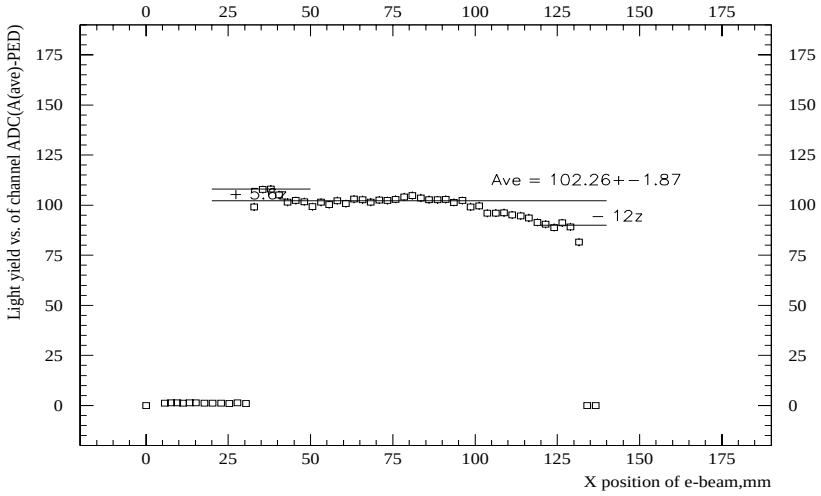


Figure II.3.4.2-1 Transverse scan of 125 mm x 132 mm and 5 mm thick tile with α - pattern of fiber groove.

This measurement has been made using 50 cm length of Bicron BCF91A WLS fiber in the α-configuration as the read-out fiber. Figure *II.3.4.2-2* shows geometry of tile and scheme of measurement.

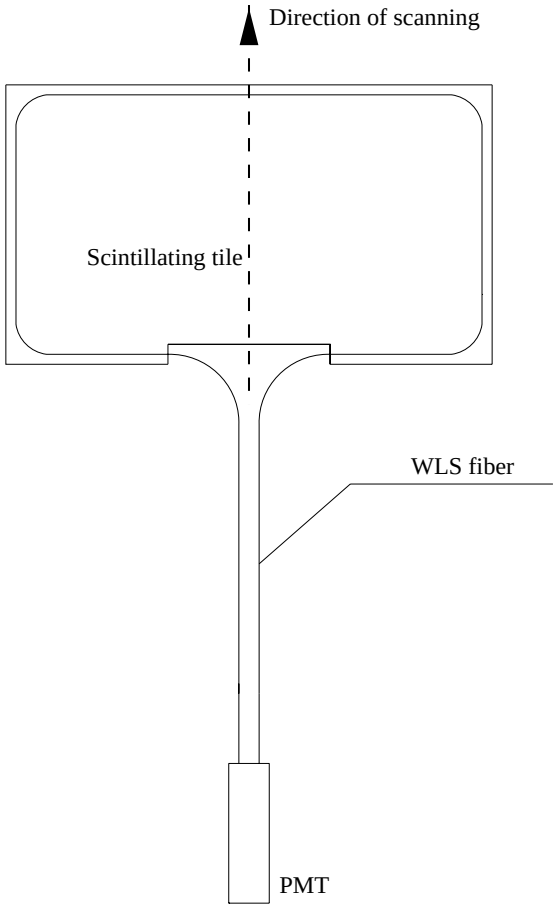


Figure II.3.4.2-2 Geometry of tile and scheme of measurement transverse uniformity.

Both the Bicron and PS scintillator with α-groove geometry show a non-uniformity of response, particularly, where the scan traverses the notch in the tile for fiber read-out. (See Figure *II.3.4.2-2*).

The PS tiles have a slightly higher non-uniformity due to their shorter attenuation length (approximately 35 cm). A simple mask will suffice to correct this non-uniformity and reduce average light yield by 30%, so the average light yield will be the same as for tile with σ-groove. Since the read-out of both fiber ends doubles the number of clear fibers and the space needed for fiber routing, we chose the tile with σ-groove read-out scheme. In this case only one end of a complete loop of the WLS fiber is connected to a clear fiber, while the other is mirrored. In order to simplify fiber routing and procedure of module assembling and mounting into a STAR magnet we exclude splicing of the green WLS to clear fiber and include optical connectors in optical design. There are two optical connectors: the first connector between green WLS fiber which embedded in tile and 3.5 m length optical cable, the second between optical cable and bundles of clear fiber that will connected to PMT. Multi-fiber optical connectors were developed by the CDF collaboration. These connectors are made via precision injection molding of mechanically

stable plastic. In this manner, all connectors are identical, and there is no need for pair matching of the connectors. The reproducibility of the optical connector transmission for many make/break operations has measured 0.6% with a transmission of 83% for a single fiber, and approximately 2% to 3% for all fibers in the connector. We will use connectors of type A for 10 fibers. The reduction of the number of read-out fibers and optical connectors lower the absolute light yield of tile/fiber system. However, combination of green multiclad WLS and clear multiclad fibers will compensate this reduction of the light output. As shown in our results, the use of multiclad Kuraray fibers will significant increase the light yield. In addition, testing at ANL of the mechanical stability of the light output using Bicron fibers indicates that Bicron BCF91A is unsuitable at the fiber bend radii encountered in routing the fibers through magnet coil.

Figure *II.3.4.2-3* shows the typical transverse uniformity of the unmasked σ-groove PS tiles from the 2x2 megatile. Figure *II.3.4.2-4* shows geometry of megatile and scheme of optical read-out system. The absolute light yield of megatile is plotted as a function of the position of the electron source. The depth of fiber groove is 2 mm. The distance of the fiber groove from the edge of tile is 1.5 mm. About 0.25 mm of the 5-mm thick scintillator are left uncut at the bottom of the grooves separating the tiles. The width of separating grooves is 1 mm. The grooves are filled with white epoxy for both structural support and light isolation. A black line is painted along the groove at the bottom surface of the scintillator, to reduce the optical cross talk, which is measured to be less than 1% per edge of the tile. The absolute light yield for this tile/fiber system is 2.28 p.e. /MIP.

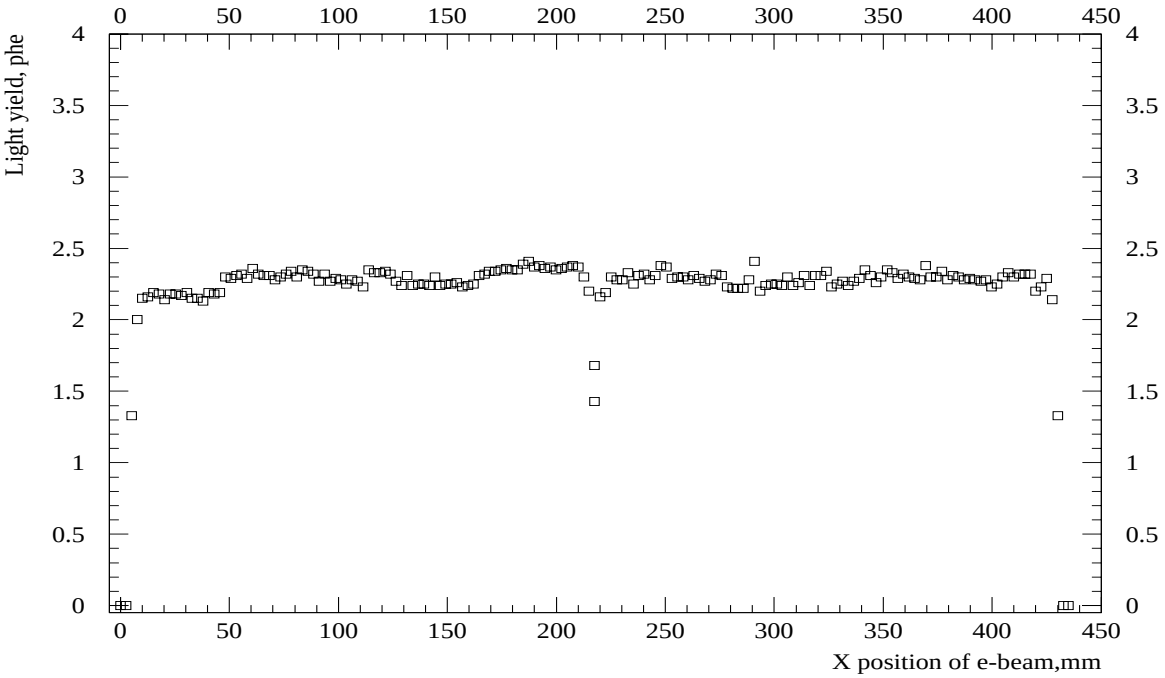


Figure II.3.4.2-3 The transverse uniformity of the two tiles (125 mm x 200 mm x 5mm) with σ-pattern of fiber groove from the 2 x megatile. The depth of fiber groove is 2 mm and the separating groove between tiles is 1 mm wide. The relative light yield of the megatile is plotted as a function of the position of electron source.

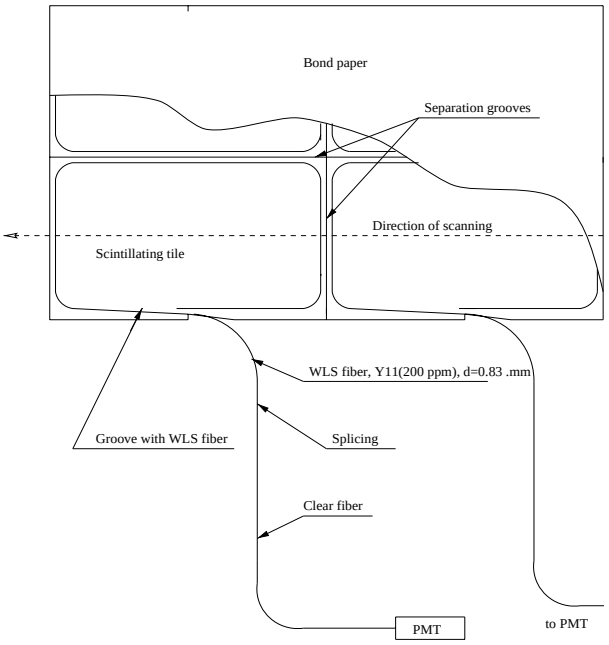


Figure II.3.4.-4 Geometry of megatile and scheme of optical read-out system

The photoelectron yield is a complex factor depending not only on the light output of the tile, light collection efficiency and fiber choice, but also on the PMT choice. For these measurements we have used Hamamatsu green extended R580-17 phototube. Measurements have also been made comparing the sensitivities of R580-17 phototube vs. the much cheaper Russian FEU115-M phototube. Initial measurements indicate that the FEU115-M is more sensitive than the R580-17 and the FEU115-M increases the light yields from the Y11 (200 ppm) green WLS fiber by 25%. Typical single-photoelectron peaks for FEU115-M and R580-17 are shown on Figure *II.3.4.2-5, II.3.4.2-6.*

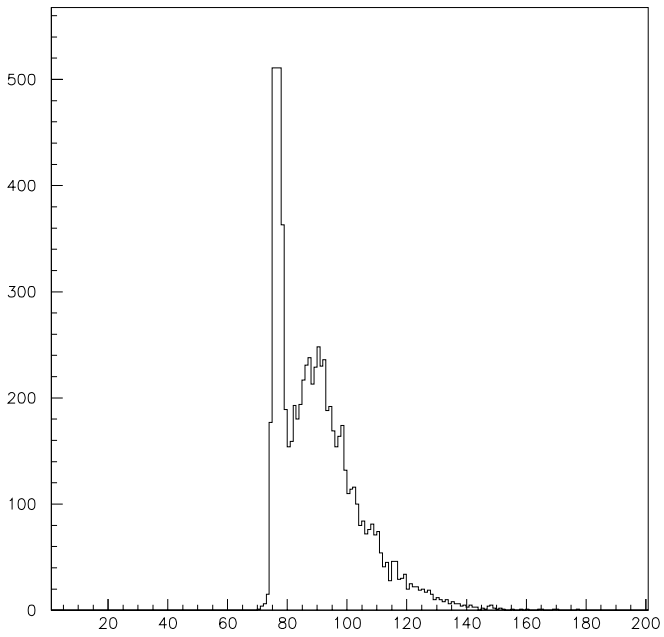

Figure II.3.4.2-5 Single photoelectron peak for phototube FEU 115-M

The uniformity over the surface of the tiles within the megatile is excellent with an rms /mean of approximately 3%, excluding the crack region. The response non-uniformity in the diagonal direction was measured to be smaller than the non-uniformity across the tile. This value is consistent with an attenuation length of PS scintillator/fiber system about 40 cm (without bond paper, the effective attenuation length is 35 cm). The measurements of uniformity and simulation [10] agree well. Our results of tile/fiber optimization

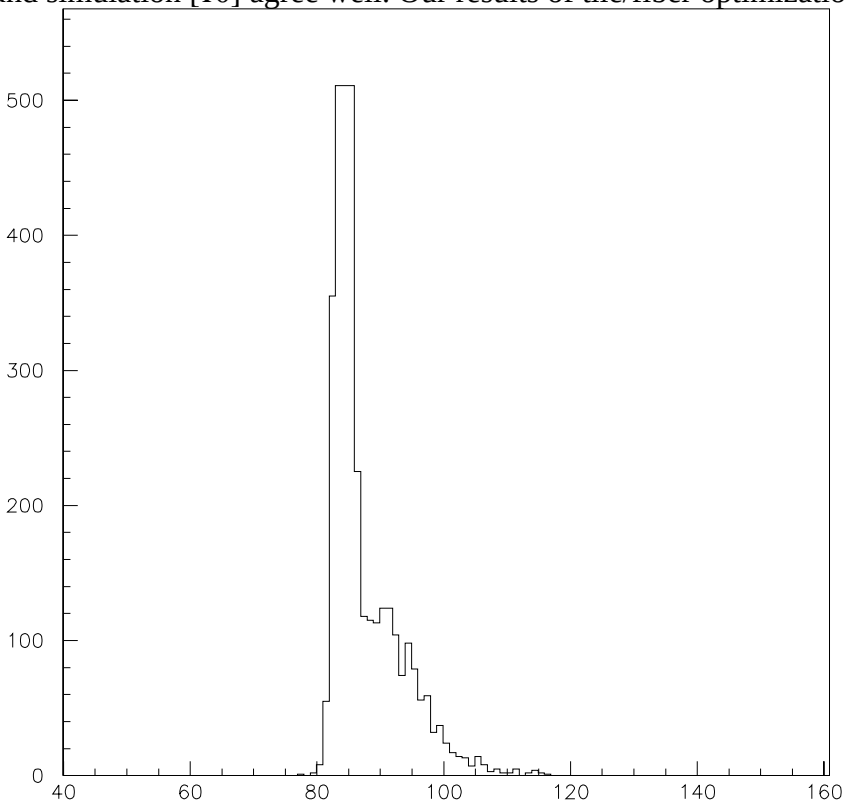

Figure II.3.4.2-6 Single photoelectron peak for phototube R580-17.

show, that for relatively small sizes of scintillating tiles with σ-groove, the Russian extrusion PS scintillator is good choice. Table *II.3.4.2-1* summarized of the design parameters of the scintillating tile for Barrel EMC of STAR. Figure *II.3.4.2-7* shows the design of optical read-out system. Our design of optical system is similar to the CDF endcap optical design.

| | |
|---|---|
| Scintillator material | PS(PSM115 scintillator) extrusion |
| Scintillator thickness | 5 mm |
| Fiber groove depth | 2 mm |
| Radius of fiber grooves | 30 mm |
| Distance of fiber groove from edge of tile | 1.5 mm |
| Tile edge treatment | White paint BC-620 |
| Tile wrapping | Bond paper |
| WLS fiber material | Kuraray Y11(200 ppm), multiclad, S-type |
| WLS fiber diameter | 0.83 mm |

Table II.3.4.2-1 Design parameters of the scintillator tile for Barrel EMC of STAR.

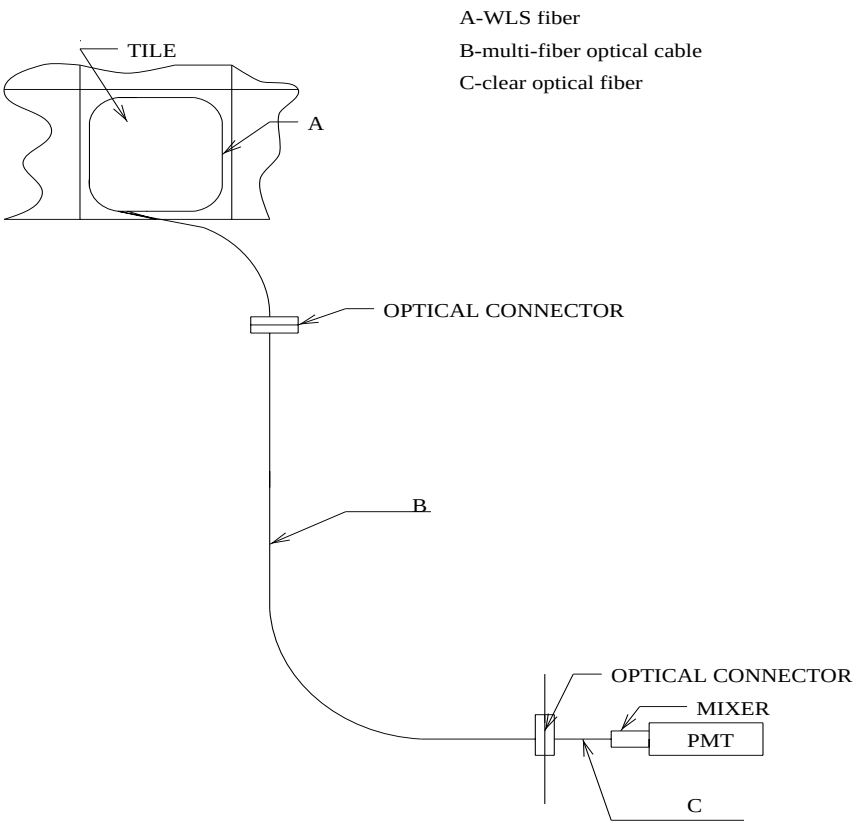


Figure II.3.4.2-7 Design of optical read-out system of Barrel EMC STAR.

### II.3.4.3 Light yield variation

For Barrel EMC with projective geometry, the tiles forming the front (inner) layers of a calorimeter are smaller than the tiles forming the back (outer) layers of the calorimeter. As we know [11] the relative light yield of different size tiles to scale with variable l/A, where l is the length of the WLS read-out fiber inside the tile and A is the area of the tile. Using this parameterization, the predicted ratio of the light yield of the front layer tiles to the back layer tiles would be 1.1. This factor 1.1 does not include the correction due to different length of clear fibers used in routing of light from optical connector inside light decoding box to PMT. This difference would be approximately equal to 100 cm. Taking the average attenuation length of clear fiber to be 10 m, the ratio of the light yield of front layer tiles to back layer tiles corrected for the different length of clear fibers would be 0.99. The scaling of the light yield of tile/fiber system with sigma-groove inside tile indicates that the response of the tiles within same readout tower can be adjusted by varying the length of the clear fibers between PMT and optical connector inside light decoding box.

The CDF Plug Upgrade group developed an independent method of equalizing the light yield of tiles. In this method, the absolute light yield of tiles in each layer was adjusted by changing the distance between the edge of the tile and the fiber groove, thus affecting the value l/A parameter. In addition, the light yield of tiles could be adjusted by extending the length of WLS fibers past the edge of tile.

Longitudinal uniformity to a level of less than 10% within each tower is significant technological issues relating to the optical system, where high performance is required. This uniformity includes contribution from: non-uniformity inside a tile, tile-to-tile variation, tile to fiber coupling, variation in fibers, variations in fiber-to-fiber coupling (optical connector) and variations of the response across the PMT photocathode. We have done detailed studies to identify the requirements on the optical system so that these variations do not contribute substantially to the constant term in the calorimeter resolution. We found that keeping the longitudinal uniformity to a level less than 10% rms within each tower is acceptable. Our studies of light variations for optical components translate to requirements:

- Tile-to-tile variations, including non-uniformity inside a tile and tile to green WLS fiber coupling: ≤ 7% in rms.
- Variations in fiber-to-fiber coupling (optical connector): ≤ 3% in rms.
- Variations in clear fibers: ≤ 3% in rms.
- Variations of the response across the PMT photocathode: ≤ 2% in rms.
- Light leakage to adjacent tiles:≤2%.

Our design of optical system is similar to the optical system of CDF End Plug calorimeter. The quality control strategy is the same as used by CDF. The thickness of each scintillating plate will be measured at several points by the IHEP (Protvino). In addition, IHEP will test scintillator plates for the attenuation length and light yield. Diameter and attenuation length of the fibers also will be well controlled. For production of fibers (cutting, polishing, and mirroring) and furnishing fibers with optical connectors we will use Fermilab and MSU facilities. The CDF End Plug calorimeter group has built several thousand tiles. The measured finished tile to tile variation of the light yield from set of 1000 tiles is found to be 6.4%. Their experience gives us confidence that the strategy will work for the Barrel EMC as well.

**II.3.4.4 Materials for optical system.**

The material used in the Barrel EMC optical system must have various properties. They must have good long-term stability, be non-demanding in handling, and easy for machining. Our baseline choice of materials are extruded PS scintillator, multiclad Kuraray Y11 (200ppm) S-type WLS fiber and multiclad Kuraray clear fiber. Some of these materials such as Kuraray multiclad green and clear fibers have been studied by the CDF and SDC groups and satisfy these requirements. Table *II.3.6.4* summarizes of the materials used in construction of Barrel EMC of STAR.

| Application | Material type |
|---|---|
| ScintillatorPS | (PSM115) extruded scintillator |
| WLS fiber | Kuraray Y11(200 ppm), 0.83 mm diam., multiclad |
| Clear fibers for cables | Kuraray, 0.93 mm diam., multiclad |
| Clear fibers for decoder box | Kuraray, 1.00 mm diam., multiclad |

Table II.3.4.4-1 Materials for optical system of Barrel EMC STAR

We concentrated on studying the extruded PS scintillator. Long-term stability of scintillating material includes variation of light output with temperature and time that must be known or controlled. In addition we have studied the effect of pressurizing the tile/fiber assemblies that can reduce absolute light output. The light yield variation can

effect the calorimeter calibration and possibly resolution. A cosmic ray test stand has been used for these studies.

The size of sample scintillator tiles was 110mm x 110mm x 5mm. Commercially available extruded PS scintillator (PSM -115 + 1%pTP + 0.01%POPOP) was used. WSU Department of Physics and Astronomy group fabricates the sample tiles. A peripheral σ-groove was machined in the tile, where green WLS fiber diameter 0.83mm was embedded. The non-polished tile edges are painted white with Bicron reflective paint. White bond paper is used on both sides of the tiles as reflector. 5 tiles are grouped into a package. The Packaged tiles were set between a pair of aluminum blocks. Light from 5 tiles re-emitted by Y11 (200 ppm) WLS fiber of 1m length is transported to a 10-stage R580-17 PMT isolated mechanically from dark box. The temperature inside the box was stabilized and was continuously monitored. There were two cosmic muon scintillating trigger counters with size 80mm x 80mm of 25mm thickness coupled by short light guide to a Hamamatsu phototubes. One muon counter was positioned in front of the package and another was positioned behind. In order to ensure minimum ionizing particle a 5 cm lead layer was insert between package of scintillating tiles and top cosmic muon scintillation counter. Figure *II.3.4.4-1* shows the scheme of the cosmic muon telescope.

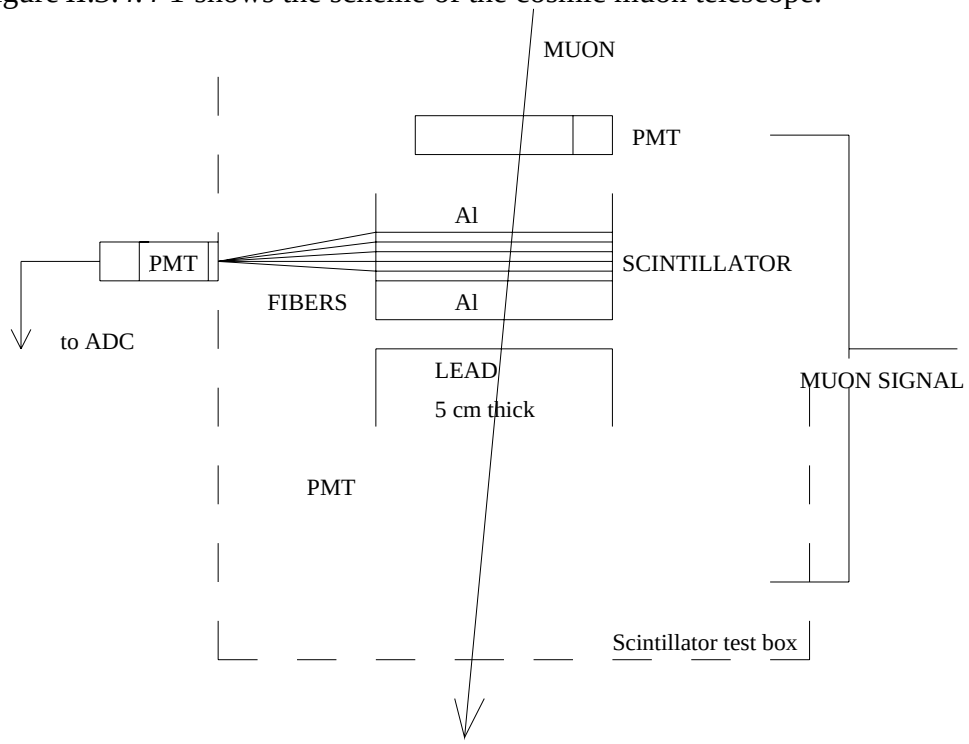


Figure II.3.4.4-1 Scheme of cosmic muon telescope.

Triggering was made with the coincidence signal of the two-muon counters. The trigger rate was 0.15 Hz. A LeCroy 2249A ADC was used for signal digitization. The ADC gate was 100 ns. Data were taken with a personal computer through CAMAC. Typically, 3000 events were collected for each point of measurements. To obtain light yield information, the spectra were fitted with a Gaussian function. Figure *II.3.4.4-2* shows the ADC pulse height spectrum from cosmic muons for tile/fiber assemblies.

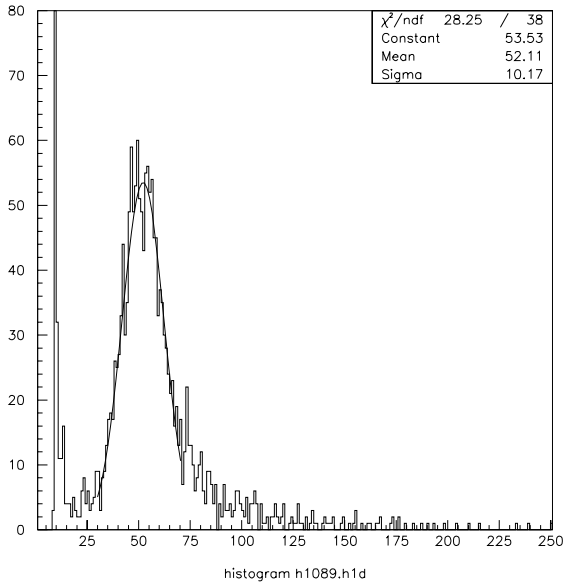


Figure II.3.4.4-2 The ADC pulse height spectrum from cosmic muons for tile tile/fiber assemblies.

### II.3.4.5 Pressurizing effect for the light yield of tile/fiber assemblies

This setup has been used to study the pressurizing effect on the light yield of tile/fiber assemblies. The packaging tiles were pressed between two aluminum blocks of 50-mm thickness. During these measurements we stabilized temperature of tile/fiber – PMT system on the level 30.1C-30.7C. Figure *II.3.4.5-1* shows the relative light yield as a function of pressure. The light yield is normalized by the yield without pressure. We have used bond paper as reflector. The light yields decrease to 1.5% at 20 PSI and to 2% at 50 PSI. Thus our measurement shows that in this case the light degradation will be 1% to 2% at the pressures encountered in our calorimeter. Most importantly, this result proves that the non-uniform pressure distribution that occurs within the stack will not influence the calorimeter performance. These results are in good agreement with the ANL result [12] that showed, for 6-mm thick polystyrene scintillator, the loss under pressure at 100 PSI is 5%.

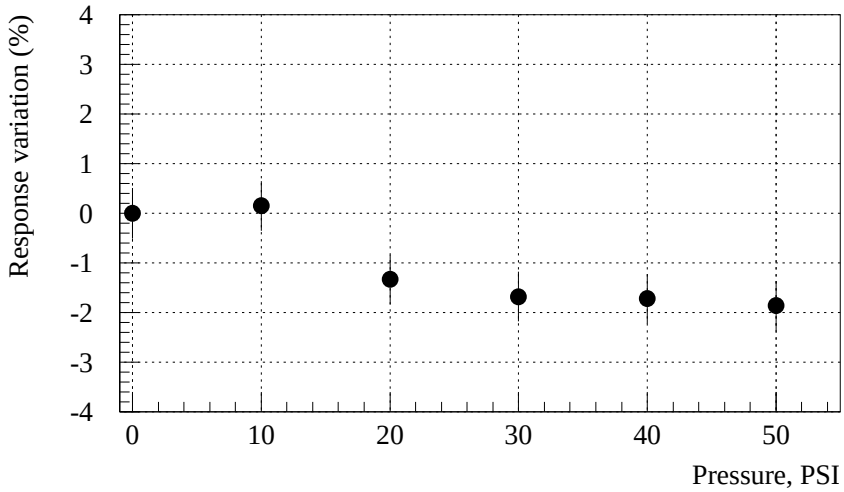

Figure II.3.4.5-1 The relative light yield as function of pressure for tile/fiber assemblies using bond paper as reflector.

### II.3.4.6 Temperature effect on scintillator tile/fiber system

We have studied the dependence of light yield of scintillator tile/fiber system on temperature. We heated samples of scintillator tiles with system of fans. The time for stabilizing of temperature inside box with accuracy 2% was typically 5-6 hours. Figure *II.3.6.6-1* presents the results of measurements. The light yield normalized by that with 24° C. The line on the figure is to guide the eye and are not fits. The light yield decreases between 3%-4% when the temperature increases from 24° C to 40° C. The large source of error ± 0.5% in these types of measurements is temperature stability of the photocathode of PMT. Temperature of PMT was continuously monitored and during measurements was 24° ± 1° C. As was established long ago, the light output of some commonly used plastic scintillators is practically temperature independent between –10° C and +20° C and has a temperature stability of about –0.125%/°C between +20° C and +60° C[13].

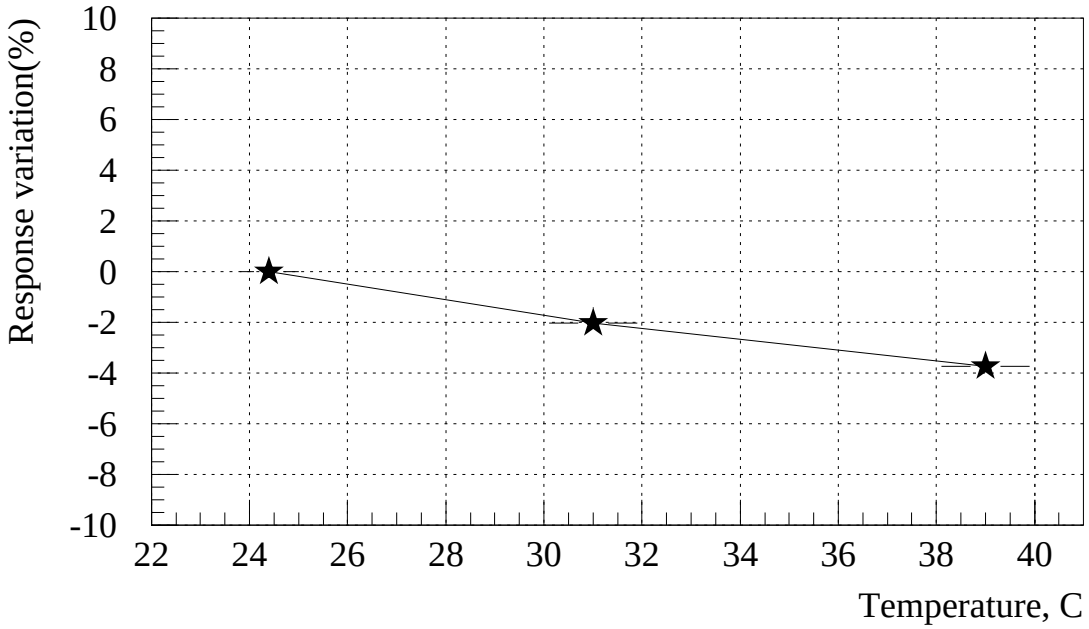


Figure II.3.4.6-1 Dependence of light yield on temperature for PS extruded scintillator.

According to our measurements, the light output stability of the PS scintillator is nearly –0.25%/C that is typical for PS scintillator[14].

### II.3.4.7 Aging

Aging is one of important issues of the Calorimeter performance. Extrusion PS scintillator has been used in many experimental setups of IHEP (Protvino) over many years and does not demonstrate any deterioration of detectors performance. To quantify this, aging of the scintillator tiles was estimated by increasing temperature action for the acceleration of chemical reactions[15].

We kept samples of extrusion PS scintillator at temperature of 50 ± 1° C during 53 days and measured light output every day. Some results are shown in Figure II.3.4.7-

1. The decrease of 8.8 % was observed after 53 days. Using result of these measurements we can evaluate possible degradation of scintillator resulting from natural aging. In accordance with our calculations, that result corresponds to the total natural aging of up to 6 years. According to our measurements the light degradation caused by natural aging should not exceed 8.8 % level after 6 years of operation.

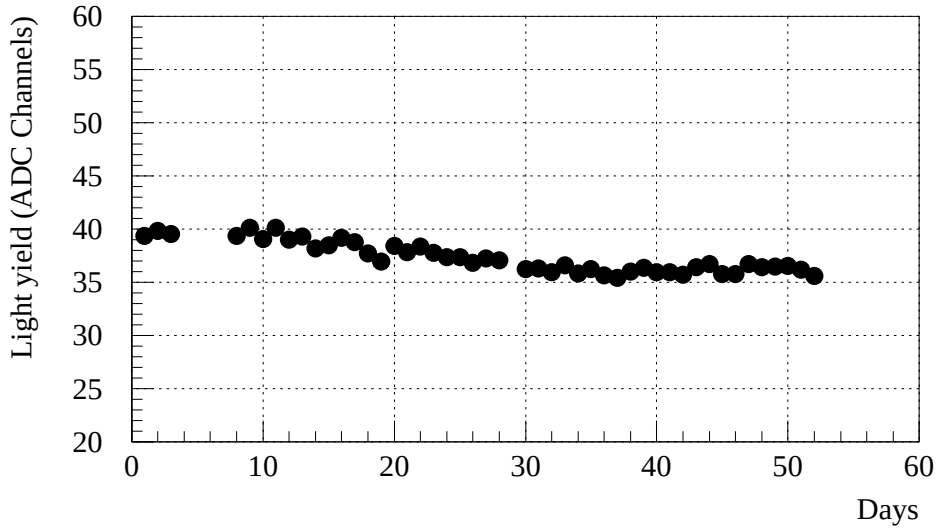


Figure II.3.4.7-1 Light degradation of PS extrusion scintillator tile/fiber system.

### II.3.4.8 PS scintillator performance in magnetic field

Experimental data have shown that the light yield output of a scintillator depends on the magnitude of the externally applied magnetic field[16,17]. The tests [18] were performed in FNAL proton area magnet facility. The samples of scintillator to be tested were installed between the poles of the magnet. Two types of scintillator based on polystyrene were tested: Kuraray SCSN38 and a scintillator prepared in Protvino, IHEP. Figure *II.3.4.8-1* presents the results of these measurements.

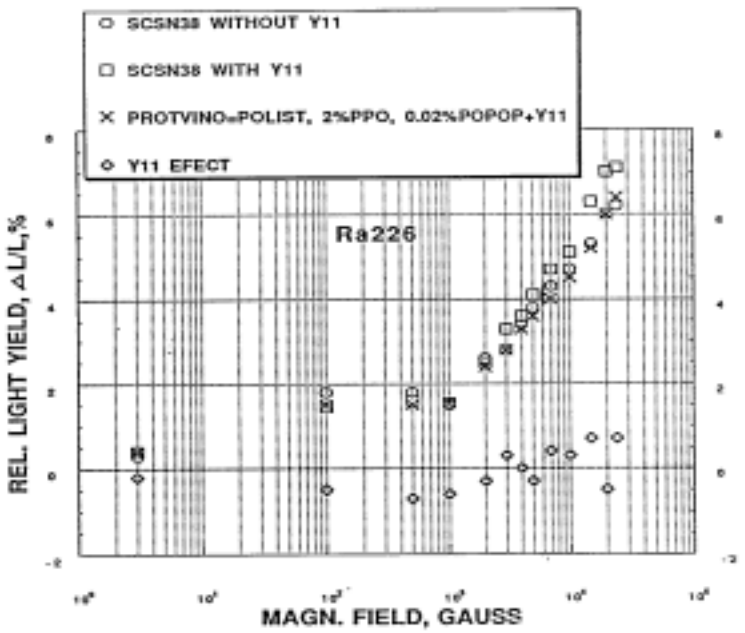


Figure II.3.4.8-1 Light yield dependence of PS scintillator from magnetic fields.

The data show the following:

1. The polystyrene based scintillator irradiated by radioactive source show a relative light yield increase up to 1-1.8% for a magnitude of magnetic field up to 0.1 kG. One can then see further growth between 1 kG and 20 kG. For the maximum STAR magnet field of 5 kG the increase in the light yield will be on the level 4%. DESY measurements with calorimeters in electron beams show same percent increasing light yield in the region of magnetic field up to 5kG in comparison with a single plate irradiated by a source.
2. The data do not depend on the magnetic field orientation. It is also not strongly dependent on the source of irradiation used (less than 1% difference for gammas or electrons).
3. There is no influence of magnetic field (for magnitude up to 140 kg) when scintillator or WLS is irradiated by ultraviolet light. Thus the light yield increase is not due to the fluors.

[1] S.Bennet et al., STAR Note SN303.

[2] O.Grachov and A.Ronzhin – Preprint IHEP 88-74, Protvino, 1988.
T.Asakawa et al., NIM, A 348(1994) 139.
S.Aota et al.,NIM, A 352(1995) 557.

[3] O.Grachov, STAR Note SN274.

[4]P.de Barbaro et al., SDC-93-407

[5]G.Apollinari et al., FERMILAB-Conf.-94/030-E(CDF).

[6]Y.Seiya et al., FERMILAB-Conf.-95/001-E(CDF)

[7]J.Freeman, FERMILAB-Conf.-96/458-E(E892)

[8] E.Bartosz et al., SDC-93-422.

[9] K.Hara et al., SDC-93-442.

[10]- V.Hagopian et al., CMS TN/96-032

[11]-P.de Barbaro et al., UR-1354.
[12]-D.G.Underwood , ANL-HEP-CP-92-94.
[13]-J.F.Camberon, Nucl.Electr.(I.A.E.A.) 1(1962) 93;
[14]-V.G.Vasil'chenko et al., Nucl.Inst. and Meth., A369(1996)55;
[15]-A.Karyukhin et al., ATLAS Note, 1 Aug. 1996.
[16]-D.Blomker et al., NIM, A311, 1992, 505.
[17]-J.Manuish et al., NIM, A312, 1992, 451.
[18]-D.Green, A.Ronzhin and V.Hagopian , FERMILAB-TM-1937, 1995.

---

[i] G. W. Foster, J. Freeman, and R. Hangstrom; Nucl. Phys. B A23(1991) 93, P. de Barbaro *et. al.*; Nucl. Instr. Meths. A315(1992) 317

[ii] P. de Barbaro *et. al.*; University of Rochester, Note UR-1371

[iii] M. Olsson; CDF/DOC/PLUG UPGR/CDFR/2582

[iv] P. de Barbaro *et. al.*; University of Rochester, Note UR-1354